Processes Controlling the Structure and Longevity of Two Quasi-Linear Convective Systems Crossing the Southern New England Coast

KELLY LOMBARDO AND BRIAN A. COLLE

School of Marine and Atmospheric Sciences, Stony Brook University, Stony Brook, New York

(Manuscript received 20 November 2012, in final form 10 May 2013)

ABSTRACT

This paper explores the structural evolution and physical processes that explain the modification of two quasi-linear convective systems (QLCSs) that encountered the densely populated New York City–Atlantic coastal region. One QLCS on 31 May 2002 traversed the Atlantic coastal boundary with little change in its intensity, producing widespread severe wind damage across New York City and Long Island. During this event, warm air advection at 925 hPa helped destabilize the layer above this level over the coastal zone, while the marine boundary layer deepened below this level. The 0–3-km line-perpendicular vertical wind shear was relatively strong, which supported ascent along the leading edge of the diabatically generated cold pool. The surface-based convective system became slightly elevated as it moved over the marine waters. In contrast, the 23 July 2002 QLCS decayed upon encountering the Atlantic coastline, despite its coincidence with a surface cold front. The most unstable CAPE values during this decaying event were 400–800 J kg^{-1} greater than the sustaining 31 May event, though the 0–3-km vertical wind shear was approximately half. Weaker shear likely contributed to limited ascent along the leading edge of the surface based cold pool, and ultimately the demise of the convective line. Sensitivity tests highlight the importance of the relationship between the cold pool and vertical shear during these two events, and illustrate the limited role of the marine layer in modifying the evolution of these two convective systems.

1. Introduction

Organized convective systems can be modified as they cross an orographic barrier or a land–water coastal boundary. Numerous studies have addressed the influence of terrain on mesoscale convective systems (MCS; e.g., Carbone et al. 2002; Ahijevych et al. 2004; Frame and Markowski 2006; Parker and Ahijevych 2007; Reeves and Lin 2007; Miglietta and Rotunno 2009; Letkewicz and Parker 2010, 2011), but fewer studies have explored the evolution of organized convective storms passing over the coastal ocean (e.g., Mapes et al. 2003; Lombardo and Colle 2010; Murray and Colle 2011) and large lakes (Bosart and Sanders 1981; Bosart and Galarneau 2005; Workoff 2010; Metz 2011). A better understanding of evolving convective systems near the coast is important for severe storm forecasting, since these are often regions of relatively dense populations.

Some studies have focused on the diurnal evolution of convection near the coast. Mapes et al. (2003) showed that a strong nighttime/morning maximum in rainfall exists over the coastal ocean of northwestern South America, with convective systems moving away from the land overnight. Murray and Colle (2011) found a similar trend over the northeastern United States, with convective systems moving eastward toward the coast during the late afternoon and evening, thus creating a nocturnal (0600–1200 UTC) maximum in convective activity over the coastal waters. However, the total frequency of convective storms over coastal waters is comparatively less than inland areas over the Northeast (Lombardo and Colle 2010; Murray and Colle 2011).

Several observational studies have highlighted the modification of convection by the Great Lakes (Changnon 1980; Bosart and Sanders 1981; Bosart and Galarneau 2005). Changnon (1980) noted the suppression of convection over the relatively cool waters of southern Lake Michigan, though this marine influence was negligible during heavy rain events associated with squall lines and cold fronts. The mesoscale convective complex that produced the July 1977 Johnstown, Pennsylvania,

Corresponding author address: Kelly Lombardo, School of Marine and Atmospheric Sciences, Stony Brook University, Stony Brook, NY 11794-5000.
E-mail: kellyann.lombardo@gmail.com

DOI: 10.1175/MWR-D-12-00336.1

© 2013 American Meteorological Society

flood temporarily weakened as it moved over the Great Lakes, and subsequently reintensified over Pennsylvania (Bosart and Sanders 1981). Similarly, during the 2003 Bow Echo and Mesoscale Convective Vortex (MCV) Experiment (BAMEX; Davis et al. 2004), a portion of an intense squall line crossing over Lake Erie decayed relatively rapidly compared to the segment of the convective line that moved over the adjacent land areas (Bosart and Galarneau 2005). During a contrasting BAMEX event, an eastward-moving quasi-linear convective system (QLCS) intensified at the western shore of Lake Michigan, weakened over the eastern portion of the lake, and reintensified as it crossed the eastern shore of the water body (Bosart and Galarneau 2005). It was hypothesized that southerly surface winds over lower Lake Michigan in conjunction with southwesterly winds over southern Michigan may have contributed to enhanced low-level convergence along the western shore of the lake, contributing to the intensification of the squall line (Bosart and Galarneau 2005).

Several recent studies have explored the influence of environmental variations across land–water boundaries on the evolution of organized convective systems (Lericos et al. 2007; Workoff 2010). For organized convective systems moving offshore and over Lake Erie, Workoff (2010) found that neither the stability of the marine layer nor the strength of the convectively generated cold pool predicted the maintenance or decay of the systems. However, a high correlation existed between weakening QLCSs and weak-to-moderate ($<15\,m\,s^{-1}$) 0–3-km ambient vertical wind shear (Workoff 2010). Similarly, Metz (2011) showed that MCSs that successfully traversed Lake Michigan were associated with a low-level jet that was $5\,m\,s^{-1}$ stronger than those that dissipated over the lake waters. This is consistent with a number of studies that have shown vertical wind shear to be important to the organization of convective systems (e.g., Weisman and Klemp 1982; Parker and Johnson 2000; Doswell and Evans 2003) as well as the maintenance of QLCSs (e.g., Rotunno et al. 1988; Weisman et al. 1988; Weisman and Rotunno 2004; Coniglio et al. 2004, 2006).

Complementary, the two-dimensional idealized numerical experiments of squall lines moving onshore from an ocean environment performed by Lericos et al. (2007) support the importance of strong low-level vertical wind shear as well. By systematically varying the magnitude ($7.5–22\,m\,s^{-1}$) and depth (2.5, 5 km) of vertical wind shear, they illustrated that for the deeper and larger shear events, shear over the land decreased as much as $7\,m\,s^{-1}$ due to increased friction over the land surface. This caused the simulated storm's updraft to tilt upshear and decay as it moved onshore. Conversely, the thermodynamic variations due to the inclusion of land had a limited influence on the convective lines in the 2D simulations (Lericos et al. 2007).

Recently, several studies have addressed the influence of the marine boundary layer on northeastern U.S. convection. Murray and Colle (2011) highlighted the greater frequency of convective storm activity along the Northeast coastal region during the late summer than late spring or early summer due to the warming of the Atlantic waters and marine layer by late summer. They also showed that convective storms in this coastal region during any part of the warm season tend to weaken more on average when the relatively cool marine air is advected northward over the coastal region, while severe weather is favored with a more westerly (offshore) low-level flow. Lombardo and Colle (2012) showed that the maintenance or decay of Northeast region QLCSs crossing over the Atlantic coastal waters is not a function of warm season month, suggesting that sea surface temperature (SST) as well as offshore most unstable convective available potential energy (MUCAPE) are not of primary importance. They showed that systems that survived over the coastal waters were associated with $3–6\,m\,s^{-1}$ more 0–3-km environmental vertical wind shear, weaker diabatically generated cold pools, and greater low-level warm air advection than the QLCSs that decayed at the coast. Conversely, those systems that decayed at the coast were collocated with a maximum in low-level frontogenesis, a mean low-level wind shear $<7\,m\,s^{-1}$, and a more intense cold pool than sustaining systems. One hypothesis is that for a QLCS to remain intact over the ocean waters, the vertical wind shear must be large enough to balance the vorticity generated by the strengthening cold pool of the maturing system to allow for upright ascent along the leading edge of the cold pool, following the arguments of Rotunno et al. [1988; Rotunno–Klemp–Weisman (RKW) theory]. Second, the source region of the air ingested into the QLCS may be important. It is hypothesized that sustaining systems ingest warm, unstable air from above the marine inversion, with warm air advection helping to destabilize the column just above the cooler marine layer contributing to an increase in elevated CAPE.

While previous studies have provided some insight into the synoptic-dynamic and thermodynamic conditions that support convection crossing the coast of a large lake or ocean, there is a lack of understanding of the processes that control the modification of QLCSs moving from inland areas to a relatively cool coastal ocean. Currently, we do not understand the source of ambient air ingested into the storms, and how this relates to the change in vertical shear and instability across the coast. In a recent study by Parker (2008), the response of QLCSs

to a gradual, nocturnal cooling of the boundary layer was explored using idealized numerical simulations. Simulated squall lines remained surface based until the boundary layer was sufficiently cooled (by >10 K), at which point the systems became elevated, forced by a bore on top of the stable layer (Parker 2008). Similarly, high-resolution simulations of convective lines moving from a well-mixed boundary layer to a shallow marine layer are needed to diagnose the physical processes contributing to the different evolutions of convective systems crossing the coastline.

To understand the physical mechanisms governing the maintenance and decay of squall lines moving over large water bodies, detailed observational and numerical analyses of two quasi-linear systems that encountered the coastal waters of the northeastern United States are provided. Section 2 describes the data and methodology used to conduct this study. Observational and numerical analyses of two contrasting storm evolutions are presented in section 3. Section 4 provides a comparison between the two events, as well as a discussion of numerical sensitivity tests. The findings of this study are summarized in section 5.

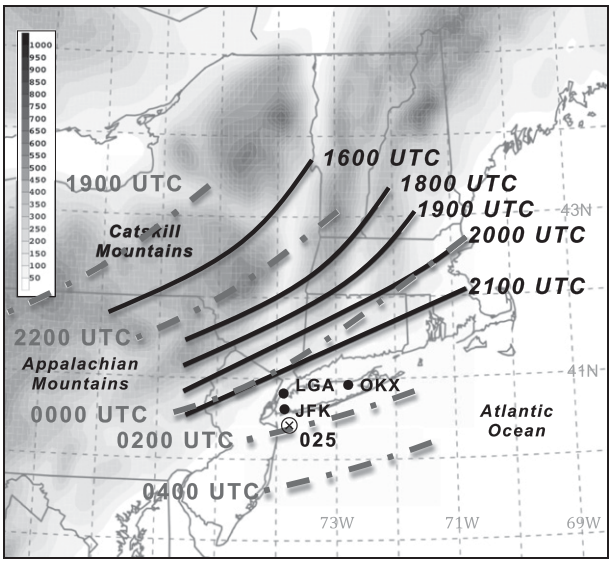

FIG. 1. The location of the leading edge of 31 May 2002 event and 23 Jul 2002 convective lines from origin to decay. The 31 May 2002 maintain event locations are marked with dark gray dash–dot line beginning at 1900 UTC and the 23 Jul 2002 decay event locations are marked with black solid line beginning at 1600 UTC. After each respective origin time (1900 UTC 31 May 2002 and 1600 UTC 23 Jul 2002), each line indicates the location of coherent quasi-linear convective system before decay (as defined in the text). Once decay occurs, no line is drawn. The approximate location of buoy 44025 is indicated by the 025, while the location of the Ambrose Light Tower (ALSN6) is denoted by the symbol ⊗. U.S. Geological Survey (USGS) terrain is shaded in meters.

2. Data and methods

a. Observational analyses

The two events selected for this study were the 31 May 2002 sustaining quasi-linear convective event and 23 July 2002 decaying quasi-linear convective event, following the classification of Lombardo and Colle (2012). For the decaying system, the radar reflectivity values decreased below 50 dBZ at the coastline, while the sustaining system maintained its reflectivity intensity of ≥50 dBZ over the ocean waters >100 km from the coastline. The locations of both decays are illustrated in Fig. 1. Once the system begins to decay, its location is no longer marked on the map. The 31 May 2002 event (dark gray dash–dot line) initially developed as a few convective cells over western New York–Pennsylvania and organized into a line by ~1900 UTC (not shown). The line moved southeastward and decayed offshore ~200 km south the southern Long Island coast at 0445 UTC 1 June 2002. In contrast, the 23 July 2002 QLCS (black solid line) moved into the Northeast domain from the west as a weak stratiform line (not shown), and developed a leading convective line at 1600 UTC over eastern New York (not shown). The convective system moved southeastward and decayed along the Atlantic coastal boundary from New Jersey northeastward to Connecticut by ~2200 UTC 23 July 2002. Therefore, the event that occurred earlier in the season successfully traversed the coastal waters more than 100 km from the coast, while the event that occurred later in the season decayed at the coastline even though the sea surface temperatures were 5°–7°C greater.

To understand the synoptic and mesoscale evolution of these two events, an observational analysis of both cases was performed using the 3-hourly North American Regional Reanalysis (NARR) at 32-km grid spacing (Mesinger et al. 2006), 1-hourly surface observations obtained from Automated Surface Observing Stations (ASOS), National Weather Service radiosonde soundings, and Aircraft Communications Addressing and Reporting System (ACARS) sounding profiles.

b. High-resolution simulations

To diagnose the physical processes contributing to the convective evolutions, the 31 May sustaining QLCS and 23 July decaying QLCS were simulated using version 3.1.1 of the Advanced Research Weather Research and Forecasting Model (ARW-WRF) core (Skamarock et al. 2008). The sustaining event was simulated from 1200 UTC 31 May to 0600 UTC 1 June 2002, while the decaying event was simulated from 0600 UTC 23 July to 0300 UTC 24 July 2002. Both case simulations utilized an outer

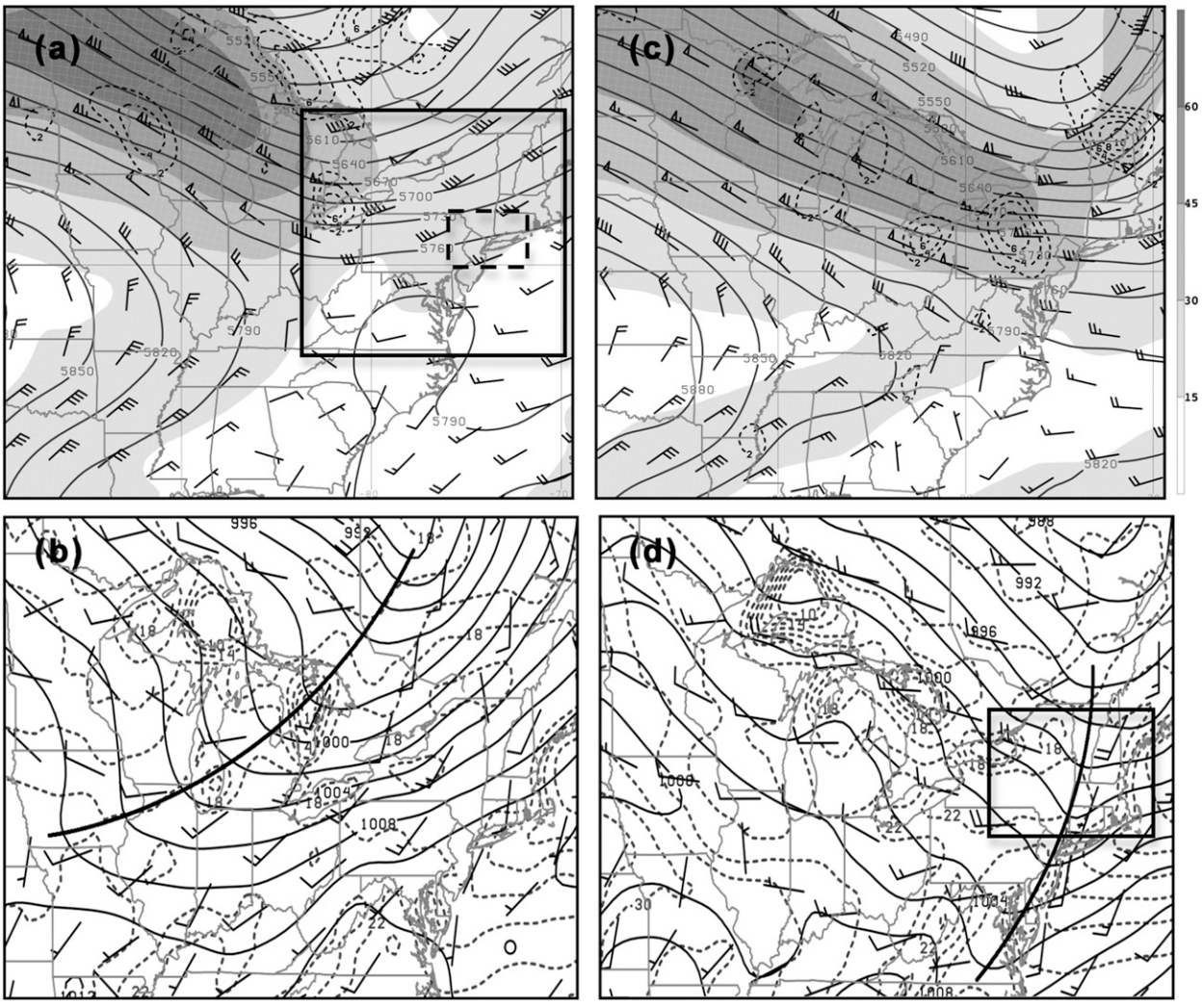

FIG. 2. The NARR (a) 300-hPa wind speed (shaded every 15 m s^{-1}), 500-hPa geopotential heights (solid every 30 m), 500-hPa **Q**-vector convergence (dashed every 2×10^{-15} K m^{-2} s^{-1}), 500-hPa winds (full barb = 5 m s^{-1}) at 1200 UTC 31 May 2002. (b) As in (a), but for mean sea level pressure (solid every 2 hPa), 2-m temperature (dashed every 2°C), and 10-m winds (full barb = 5 m s^{-1}). (c) As in (a), but at 0000 UTC 1 Jun 2002. (d) As in (b), but at 0000 UTC 1 Jun 2002. The solid box (dashed box) in (a) marks the 2-km (500 m) WRF domain, and the box in (d) marks the location of the surface analysis in Fig. 3a. The black solid line in (b),(d) marks the location of the surface cold front.

domain at 2-km grid spacing centered over the Northeast, with a 500-m inner nest centered on the New York City–Long Island region (i.e., Fig. 2a) using a one-way nest interface. The WRF used 38 vertical levels, with 13 levels in the lowest 1 km. The 32-km NARR was utilized for the initial atmospheric, sea surface temperature, soil conditions, and lateral boundary conditions.

Several simulations were conducted using different microphysical schemes, planetary boundary layer (PBL) schemes, and land surface models (LSM) to obtain the most accurate simulations of the two events. The simulations presented in this paper used the Morrison microphysical scheme (Morrison et al. 2009), the Mellor–Yamada–Nakanishi–Niino Level 2.5 (MYNN2.5; Nakanishi and Niino 2006) PBL, as well as thermal diffusion LSM. The double-moment Morrison microphysical scheme (Morrison et al. 2009) most accurately reproduced the overall intensity and structure of the two QLCSs, including the leading convective line and trailing stratiform precipitation. Morrison et al. (2009) showed that the use of a double-moment scheme, which predicts both mixing ratios and number concentrations of precipitation species, more accurately produces widespread trailing stratiform precipitation in linear convective systems compared to single-moment schemes.

The Mellor–Yamada–Nakanishi–Niino Level 2.5 (MYNN2.5; Nakanishi and Niino 2006) PBL as well as the thermal diffusion LSM produced the most accurate

surface fields, boundary layer structure, as well as the large-scale synoptic patterns. The Mellor–Yamada–Janjic (MYJ; Janjic 1990) PBL scheme produced surface temperatures that were 1°–4°C too cool, while the ambient winds in the Yonsei University (YSU; Hong et al. 2006) PBL scheme were too weak (~2.5 m s^{-1}; ~5 kt) for the 31 May case. The YSU boundary layer was too dry for the 23 July 2002 event, which caused an unrealistic reduction in instability, while the MYJ and the MYNN2.5 both reproduced more a realistic boundary layer. However, the MYNN2.5 was used for both the 23 July and 31 May events for consistency.

3. Case study results

a. 31 May 2002 event

1) SYNOPTIC AND MESOSCALE EVOLUTION

At 1200 UTC 31 May 2002, approximately 12 h before the QLCS encountered the Atlantic coastline, a 500-hPa trough was centered over the eastern Great Lakes, with a 60–75 m s^{-1} jet at 300 hPa extending southeastward into the base of the upper-level trough (Fig. 2a). Meanwhile, a surface low pressure system was situated over James Bay in Canada ~800 km north of Lake Ontario, with a trailing cold front extending southwestward through Lake Huron toward Iowa (Fig. 2b).

By 0000 UTC 1 June 2002, the 500-hPa trough axis was over eastern New York (Fig. 2c), which is similar to the composite position of the midlevel trough axis for sustaining events in Lombardo and Colle (2012, their Fig. 8d). There was 500-hPa **Q**-vector convergence over eastern Pennsylvania and western New York (6×10^{-15} K m^{-2} s^{-1}) moving toward coastal region at this time, indicating the presence of quasigeostrophic (QG) forcing for ascent (Fig. 2c). The magnitude of the 300-hPa jet increased to ~30 m s^{-1} over the coastal zone, located under the jet exit region (Fig. 2c). The surface low moved eastward to ~900 km north of the Vermont–Canada border, with the surface front in the NARR extending south-southwestward through eastern New England and New Jersey (Fig. 2d).

Closer inspection of the surface observations at 2100 UTC 31 May highlights the important mesoscale features during this event (Fig. 3a). The surface cold front was over central Pennsylvania extending northeastward into central New York, with a prefrontal trough located ~200 km to the east (Fig. 3a). Initially, the convective line organized along this cold front 2 h prior at 1900 UTC 31 May (Fig. 1), but subsequently moved east of the front becoming collocated with this prefrontal trough by 2345 UTC 31 May. The 2-km WRF realistically simulated the position of the surface cold front and prefrontal

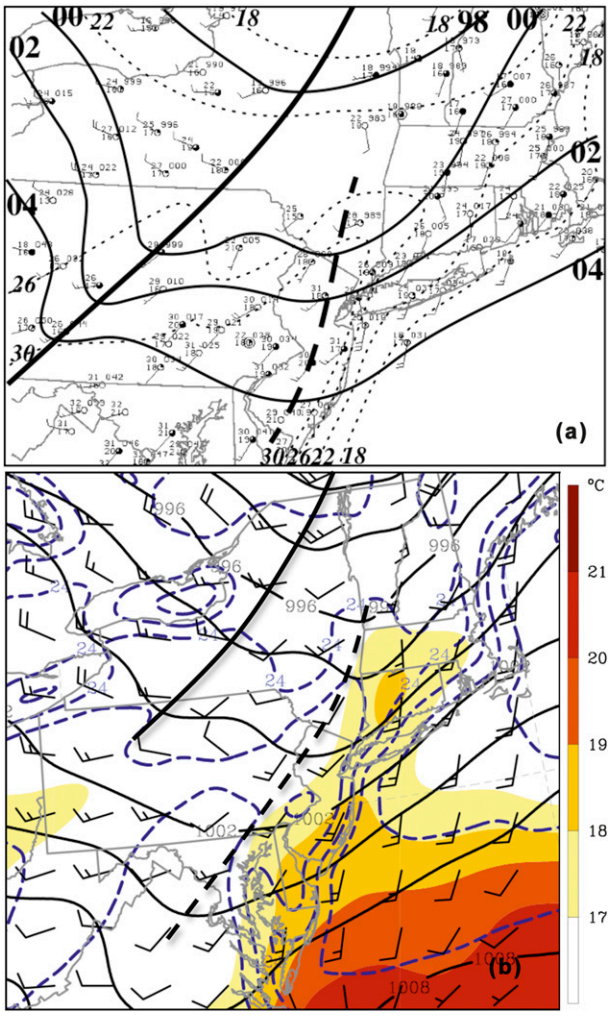

FIG. 3. (a) Manual surface analysis at 2100 UTC 31 May 2002 showing MSLP (solid every 2 hPa), temperature (dashed every 4°C), dewpoint (°C), and winds (full barb = 10 kt, where 1 kt = 0.5144 m s^{-1}). The locations of the cold front and prefrontal trough are given by the thick solid line and dashed line, respectively. (b) The 2-km WRF MSLP (solid every 2 hPa), 2-m temperature (dashed blue every 3°C), 2-m dewpoint (shaded every 1°C beginning at 17°C), and 10-m winds (full barb = 5 m s^{-1}) at 2100 UTC 31 May 2002 (9-h forecast). The locations of the cold front and prefrontal trough are given by the thick solid line and dashed line, respectively.

trough at the surface over the northeastern United States at 2100 UTC 31 May (Fig. 3b). The WRF also reproduced the thermal ridge in the Appalachian lee, with a maximum temperature of 29°C over New Jersey (Fig. 3b), which was ~1°C cooler than observed (Fig. 3a). The cooler sea surface temperatures to the east of the thermal ridge created a prominent surface baroclinic zone along the Atlantic coastline in both the observations and the WRF (Figs. 3a,b). A narrow corridor of relatively moist air (dewpoints 17°–18°C) was located within this

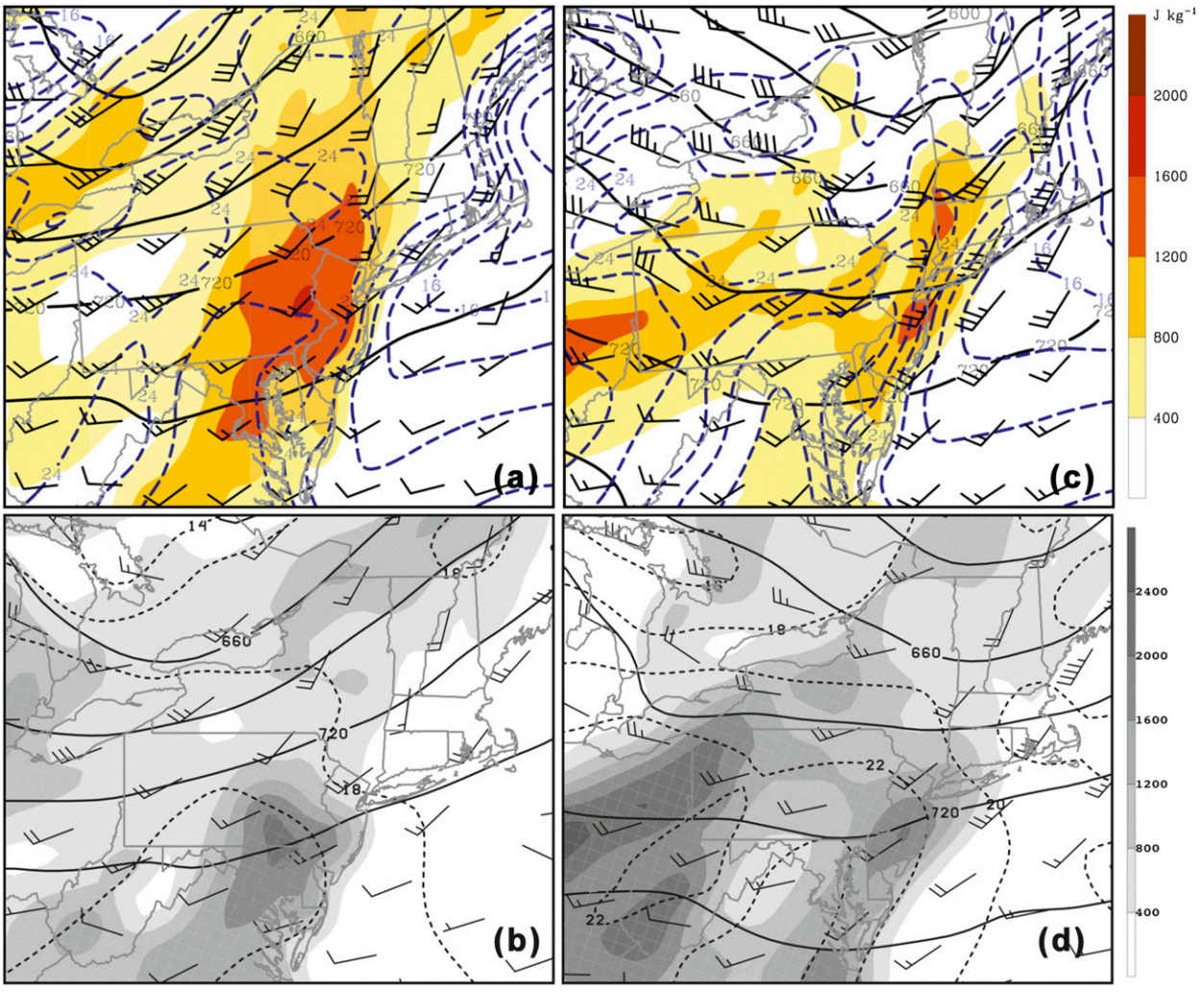

FIG. 4. (a) The 2-km WRF MUCAPE (shaded every 400 J kg^{-1}), 925-hPa geopotential heights (solid every 30 dam), 925-hPa temperature (dashed every 2°C), and 925-hPa winds (full barb = 5 m s^{-1}) at 1500 UTC 31 May 2002. (b) NARR MUCAPE (shaded every 400 J kg^{-1}), 925-hPa geopotential heights (solid every 30 dam), 925-hPa temperature (dashed every 2°C), and 925-hPa winds (full barb = 5 m s^{-1}) at 1500 UTC 31 May 2002. (c) As in (a), but at 2100 UTC 31 May 2002. (d) As in (b), but at 2100 UTC 31 May 2002.

coastal baroclinic zone from New Jersey and Long Island northward into Connecticut and Massachusetts (Figs. 3a,b,). The WRF dewpoints were ~1°C less than observed in localized regions such as western Connecticut.

2) INSTABILITY AND WIND PROFILE

At 1500 UTC 31 May, ~9 h before the convective line crossed the Atlantic coast, WRF MUCAPE was 1600–2000 J kg^{-1} over eastern Pennsylvania and western New Jersey. MUCAPE values decreased from 800 to 0 J kg^{-1} moving eastward from eastern New York–New Jersey, western Connecticut to Long Island, and eastern Connecticut to Rhode Island (Fig. 4a). The NARR had a similar MUCAPE distribution, though the MUCAPE maximum was 400 J kg^{-1} greater and located ~150 km to the southwest of the WRF maximum (Fig. 4b). Over New Jersey, western Connecticut, southern New York, and Long Island, 925-hPa warm air advection was occurring (Figs. 4a,b), which was evident in the veering winds from the surface to 900 hPa at John F. Kennedy International Airport (JFK) (Fig. 5a; see Fig. 1 for location). Surface winds were southerly at 10.5 m s^{-1} and veered to west-southwesterly at 13 m s^{-1} at the top of the planetary boundary layer (PBL) at JFK (Fig. 5a).

By 2100 UTC 31 May, the ongoing 925-hPa warm air advection over the coastal region helped increase MUCAPE values to 400–1200 J kg^{-1} over Long Island and Connecticut (Figs. 4c and 5b), with NARR instability as much as ~400 J kg^{-1} larger than the WRF, especially over southern New Jersey (Fig. 4d). This increase in

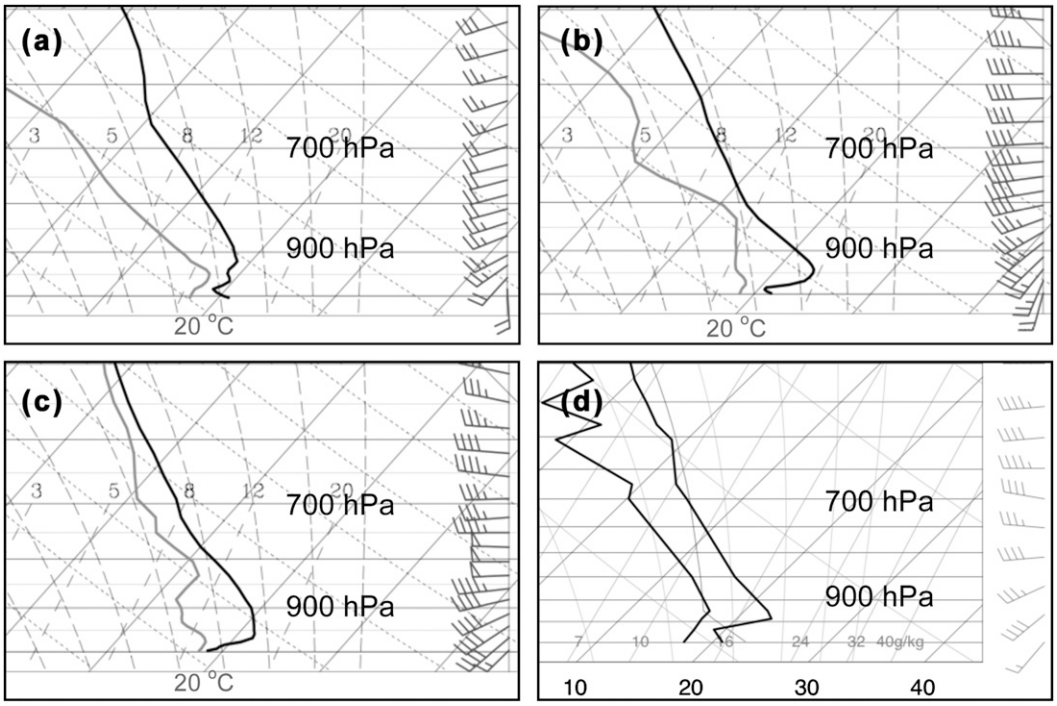

FIG. 5. WRF sounding from the 500-m domain at JFK at (a) 1500 UTC 31 May 2002 and (b) 2100 UTC 31 May 2002. (c) As in (a), but for 0000 UTC 1 Jun 2002 at OKX. (d) As in (c), but for observed sounding at 0000 UTC 1 Jun 2002.

instability was evident in the evolving local thermodynamic vertical profiles, such as at JFK. At 1500 UTC, the JFK temperature at 925 hPa, the level of maximum warm advection, was ~18°C, with a 925–800-hPa lapse rates of ~5°C km^{-1} (Fig. 5a). By 2100 UTC, the temperature within the 1000–850-hPa layer increased, with the greatest change (4°C) near the 950–925-hPa layer (Fig. 5b), steepening the 925–800-hPa lapse rates to ~8°C km^{-1}. Winds at the top of the PBL increased to 12–15 m s^{-1} from the southwest (Fig. 5b).

At KOKX over eastern Long Island (see Fig. 1 for location) at 0000 UTC 1 June, the temperatures were also warmest between 925 and 950 hPa in both the simulated (Fig. 5c) and observed (Fig. 5d) soundings, though the WRF profile was 2°–3°C too cool between the surface and 850 hPa. Cooler model boundary layer temperatures may have resulted in lower model instability compared to observations (Figs. 4c,d). The top of the marine inversion was at ~940 hPa (~750 m deep), through which the southwesterly winds increased from 7.5 m s^{-1} near the surface to ~20 m s^{-1} at the top of the marine layer.

3) RADAR AND QLCS EVOLUTION

Figure 6 illustrates the observed radar and WRF precipitation mixing ratio evolution as the QLCS encountered the coastline. At 2258 UTC 31 May, the observed QLCS was ~75 km north-northwest of Long Island. Radar reflectivities approached 70 dBZ within the convective cores, with little trailing stratiform precipitation behind the leading convective line. By 0043 UTC 1 June, the QLCS reached the coast, with radar reflectivity values increasing in the southern New York–New York City region, resulting in a continuous band of radar reflectivity values >35 dBZ at this time (Fig. 6b). Subsequently, the convection moved south of Long Island over the Atlantic coastal waters at 2215 UTC 31 May and 0000 UTC 1 June (Figs. 6c,d).

The WRF at 2-km and 500-m grid spacing realistically simulated the evolving QLCS structure (Figs. 6e–h), though the simulated linear system was slower than the observed, with the simulated convection ~75 km north-northwest from the coast at 2215 UTC (Fig. 6e). By 2345 UTC (Fig. 6f), the WRF QLCS moved offshore, intensifying south of western Long Island by 0030–0100 UTC (Figs. 6g,h). This intensification occurred in an area of enhanced low-level convergence (not shown) between the QLCS outflow and the 15–20 m s^{-1} southwesterlies 100 m MSL. The observed QLCS was most intense just south of western and central Long Island around this time as well.

Figure 7 presents cross sections of the QLCS as it interacted with the Atlantic marine environment. Variables displayed in the cross sections are averaged over

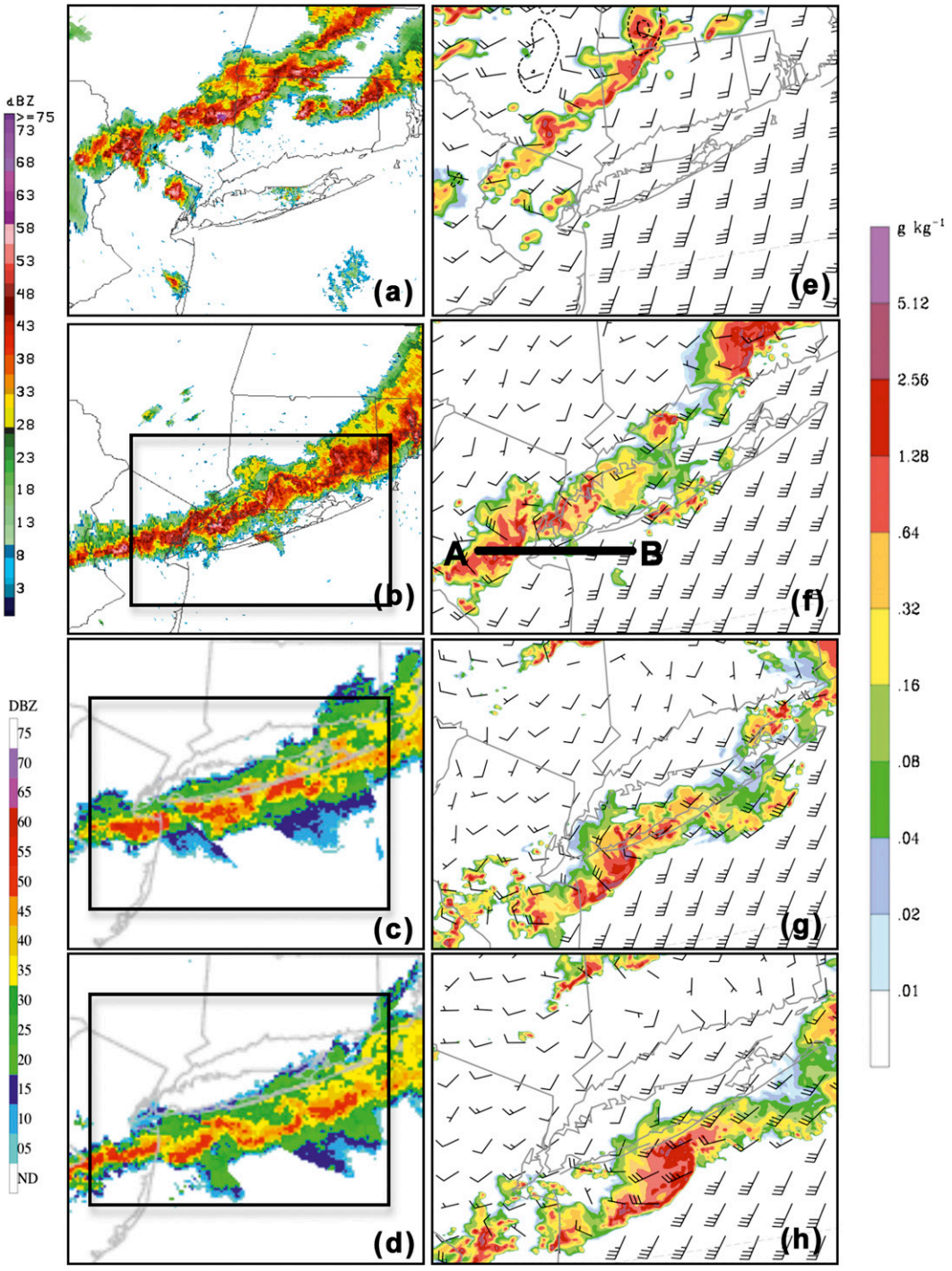

FIG. 6. Observed reflectivity from the OKX Weather Surveillance Radar-1988 Doppler (WSR-88D) (0.48° elevation scan) at (a) 2258 UTC 31 May 2002 and (b) 0043 UTC 1 Jun 2002. Weather Services International (WSI) National Operational Weather Radar (NOWrad) radar reflectivity at (c) 0145 UTC 1 Jun 2002 and (d) 0215 UTC 1 Jun 2002. The WRF total precipitation mixing ratio (shaded in g kg^{-1}) and 100 m winds (full barb = 5 m s^{-1}) are shown for 2-km domain at (e) 2215 UTC 31 May (10.25 h), for 500-m domain at (f) 2345 UTC 31 May (11.75 h), (g) 0030 UTC 1 Jun (12.5 h), and (h) 0100 UTC 1 Jun (13 h). WSI NOWrad radar reflectivity was used in place of level 2 because of missing archived data after 0100 UTC 1 Jun 2002. The box outline in (b) highlights the location of the WRF image in (f)–(h), respectively.

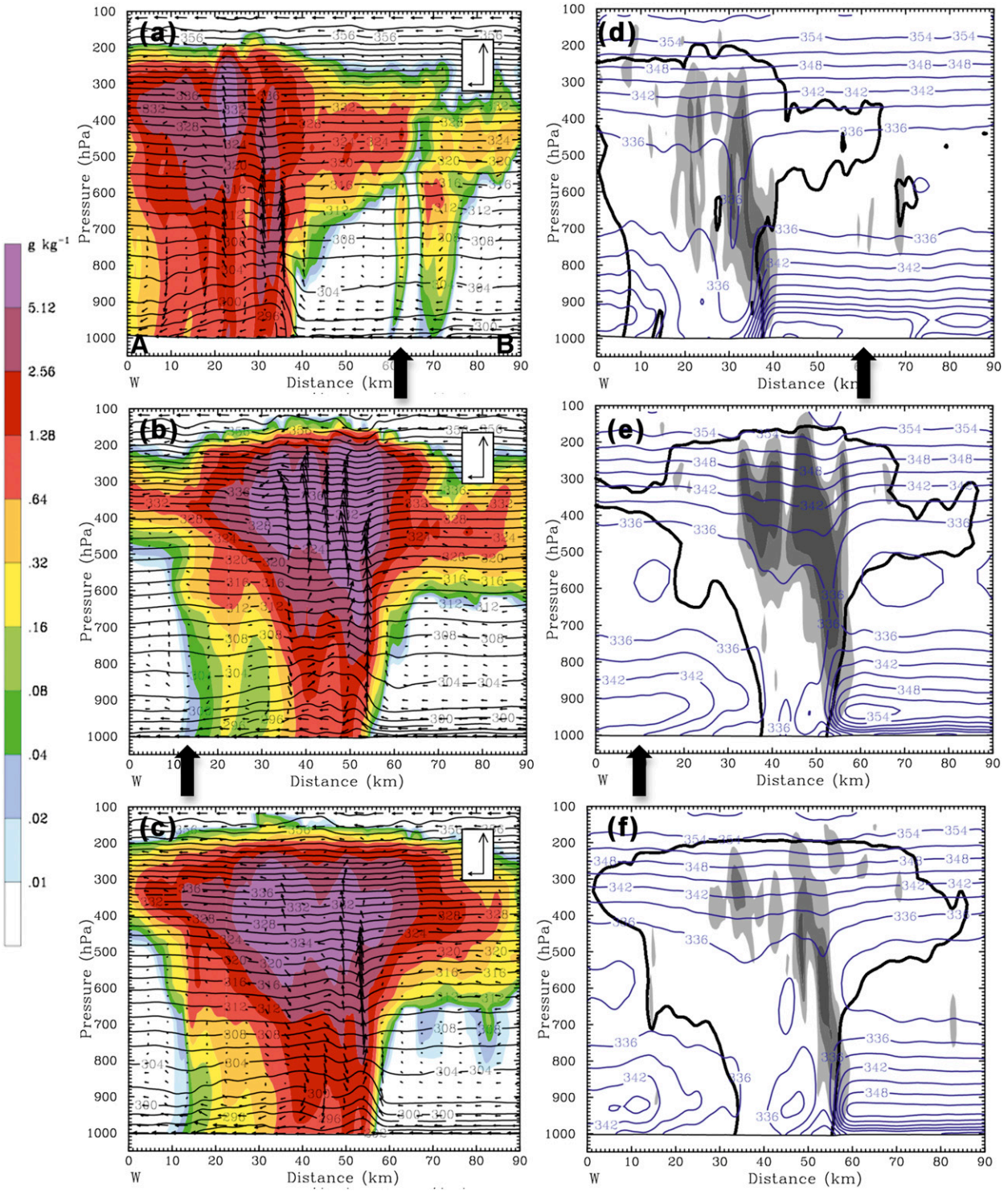

FIG. 7. 500-m WRF cross section AB (labeled in Fig. 6f) averaged over 2-km width at (a) 2345 UTC (11.75 h) 31 May 2002, (b) 0030 UTC (12.5 h) 1 Jun 2002, and (c) 0100 UTC (13 h) 1 Jun 2002. (a)–(c) Precipitation mixing ratio (shaded, g kg^{-1}), θ (black every 2 K), storm-relative circulation vectors (storm motion east at 23.5 m s^{-1}) with the horizontal reference vector of 25 m s^{-1} and vertical reference vector of ~6.5 m s^{-1}. (d)–(f) Vertical motion (shaded every 3 m s^{-1}, beginning at 1 m s^{-1}), precipitation mixing ratio (black, 0.64 g kg^{-1}), and θ_{es} (blue every 3 K). The cross-sectional orientation is marked with a black line in Fig. 6f. The coastline location is marked by an arrow.

TABLE 1. Cold pool and environmental parameters corresponding to the cross-sectional times in Figs. 7 and 15; H is the cold pool depth (km AGL) from the surface to where $B = g(\theta_v'/\overline{\theta}_v - q_c)$ becomes >0, θ_v' is the virtual potential temperature associated with the cold pool, c is the theoretical speed of the cold pool ($m\,s^{-1}$) defined by Eq. (1) through depth H, and Δu is the magnitude of the environmental vertical wind shear normal to the cold pool through the depth H. For the elevated parameters, $B = g(\theta_v'/\overline{\theta}_v - q_c)$ is >0 near the surface at these two times, so H is defined as the layer where $B = g(\theta_v'/\overline{\theta}_v - q_c) < 0$, with c and Δu calculated through the depth of this nonsurface-based layer.

Time	H	θ_v'	C	Δu	$c/\Delta u$
2345 UTC 31 May 2002	2.2	−4.2	25.7	17.2	1.5
0030 UTC 1 Jun 2002	2.1	−1.9	18.0	11.1	1.6
Elevated	1.9	−3.0	21.0	5.8	3.6
0000 UTC 1 Jun 2002	2.1	−2.4	20.6	10.7	1.9
Elevated	2.0	−3.2	22.5	7.6	3.0
2115 UTC 23 Jul 2002	2.7	−1.2	15.3	10.2	1.5
2200 UTC 23 Jul 2002	2.1	−2.5	19.4	7.0	2.7
2300 UTC 23 Jul 2002	3.5	−1.4	17.8	6.2	2.9

a 2-km-wide band, centered along and parallel to the orientation of cross section AB (Fig. 6f); therefore, variables displayed are not representative of a single slice. The black line labeled AB in Fig. 6f illustrates the orientation of the cross sections, which was taken parallel to the west to east movement of the most robust section of the QLCS. Environmental and cold pool parameters were calculated and averaged over the 2-km-wide cross section as well, following the methods of Trier et al. (2006) and illustrated in Table 1. The depth of the cold pool H is defined as the level over which the cold pool buoyancy, $B = g(\theta_v'/\overline{\theta}_v - q_c)$, is <0. The virtual potential temperature perturbation θ_v' is the difference in the 20-km along-line-averaged θ_v within the cold pool and similarly averaged θ_v (referred to as $\overline{\theta}_v$) within the ambient environment beginning 10 km downstream of the cold pool, both calculated through depth H. The contribution of all condensate is included in q_c (Trier et al. 2006).

While the QLCS was still over inland New York–New Jersey at 2345 UTC (Fig. 6f), the leading edge of the convection was collocated with a 2.2-km-deep (surface–800 hPa) cold pool (Fig. 7a; Table 1), with a virtual potential temperature perturbation of 4.2 K (Table 1). The cooler air associated with the marine boundary layer is evident in the right portion of the domain, with a 2–3-K decrease in θ below 960 hPa (lowest 400 m; Fig. 7a). There is ascent ($\sim$7 $m\,s^{-1}$) along the leading edge of the cold pool (Fig. 7b), indicating that gust front lifting along the leading edge of the QLCS was adequate to lift parcels to their 850-hPa ($\sim$1.5 km) level of free convection (LFC; not shown). The system was approaching a region of conditional instability from the surface to $\sim$550 hPa ($\sim$4.5 km MSL; Fig. 7e).

By 0030 UTC 1 June as the QLCS moved over the coastal waters, θ values along the leading edge of the 2.1-km-deep cold pool (Fig. 7c; Table 1) became comparatively lower than the surrounding environment, causing the θ surfaces to appear raised and resemble an atmospheric bore (Parker 2008). The LFC at this time was $\sim$800 hPa ($\sim$2 km; not shown), indicating that the cold pool was capable of lifting parcels to saturation. At this time, there was no surface-based CAPE available (not shown), and the QLCS realized the elevated instability of $\sim$1000–1500 $J\,kg^{-1}$ (not shown). Furthermore, B was >0 in the lowest 200 m, indicating that the relative strength of the cold pool and its contributions to vertical motion was effectively zero in this layer (Parker 2008). Therefore, the *elevated* cold pool parameters were recalculated in this 200–2100-m layer, with a θ_v' value of 3.0 associated with the cold pool (Table 1).

A layer of conditional stability between the surface and $\sim$930 hPa ($\sim$750 m; Fig. 7e) highlights the depth of the stable marine layer. The stronger region of ascent (>4 $m\,s^{-1}$) was visible at 875 hPa (1.2 km MSL), which is above the marine layer (Fig. 7d), and this lifting is $\sim$500 m higher than at 2345 UTC (Fig. 7b). The 0–3-km storm-relative line-perpendicular ambient vertical wind shear, defined as the vector wind difference between 0 and 3 km, was 15–20 $m\,s^{-1}$, which is greater than the mean environmental value for sustaining QLCS events (13.5 $m\,s^{-1}$; Lombardo and Colle (2012). Thirty minutes later at 0100 UTC, the convective line remained robust as it moved over the Atlantic waters (Fig. 7c). With the LFC still $\sim$800 hPa (2 km), the height of the cold pool (2.1 km; Table 1) was sufficient to lift parcels to their LFC and realize the 800–1400 $J\,kg^{-1}$ of MUCAPE above the stable boundary layer (Fig. 7f).

Forward trajectories calculated every second (interpolated from 30-s 500-m WRF output) were launched at multiple levels to ascertain the source of air ingested into the bowing segment of the QLCS as it moved eastward over the Atlantic waters. Trajectories were released at 0030 and 0100 UTC 1 June and run for 30 min. While hundreds of trajectories were launched, only a representative subset are shown for those released at 10 m (red),

100 m (green), and 500 m (blue) to simplify the interpretation (Fig. 8). Figures 8a,b,d,e illustrate the trajectories as well as vertical cross sections of precipitation mixing ratio averaged over a 2-km width along the plane of cross sections CD, C′D′ and GH, G′H′ (Figs. 8c,f). All trajectories were launched ahead of the QLCS parallel to the southwest–northeast-oriented QLCS. Since the cross sections are two dimensional, it falsely appears as though several trajectories were released behind the QLCS.

At 0030 UTC 1 June as the QLCS encounters the marine layer (Fig. 8c), trajectories from all levels were successfully ingested into the storm's updrafts, rising to ~9–11 km (Figs. 8a,b). Air parcels were initially carried north-northeastward by the prevailing boundary layer winds (Fig. 6g), until they were ingested into the convective storm (Figs. 8a,b). By 0100 1 June when the QLCS was located farther over the coastal waters (Fig. 8f), trajectories originating at 10 m rose to only ~2 km, though the majority (85%) remained below 500 m (Figs. 8d,e). Those trajectories released at 100 and 500 m still rose into the updrafts (Figs. 8d,e), indicating that the QLCS was no longer surface based, though trajectories below the surface-based inversion were ingested into the storm. This implies that the QLCS became slightly elevated, though not completely above the marine layer, as parcels within the upper boundary layer were successfully lifted to their LFC and thus participated in convective processes.

b. 23 July 2002 event

1) SYNOPTIC AND MESOSCALE EVOLUTION

At 1200 UTC 23 July, a 500-hPa trough was located over the eastern Great Lakes, with **Q**-vector convergence ~500 km north of the northeastern United States (Fig. 9a). The 300-hPa jet core (~60 m s^{-1}) was over Quebec, Canada, with a secondary jet maximum over the north central tier of the United States. At the surface, a low pressure system was over eastern Quebec, with a trailing cold front extending southwestward through western New York and the Great Lakes (Fig. 9b). Within 4 h, convection organized along this surface baroclinic zone (Figs. 1 and 9b).

By 2100 UTC, the 500-hPa shortwave moved eastward, bringing weak **Q**-vector convergence (~4 × 10^{-15} K m^{-2} s^{-1}) over Lake Erie and southern Quebec, placing the northeast in the confluent jet entrance region of the 500-hPa flow (Fig. 9c). The limited midlevel QG forcing over the coastal region is consistent with the composite of decaying QLCSs in Lombardo and Colle (2012, see their Fig. 5d). The 300-hPa jet remained along the New England–Canadian border (Fig. 9c), contributing little to vertical motions along the coast. The surface cold front was downstream of the QG forcing, ~50–100 km inland of the northeast coastline (Fig. 9d).

Figure 10 provides a detailed analysis of the evolving frontal boundary as it moved toward the coast. At 1800 UTC, the surface cold front extended from central Pennsylvania northeastward through central New England, with a secondary region of baroclinicity along the coast (Fig. 10a). By 2100 UTC, the frontal boundary merged with the coastal baroclinic zone, while the surface pressure trough weakened. A maximum in frontogenesis from 900 to 700 hPa was associated with the surface baroclinic zone, indicating that there was frontogenetical forcing present to support ascent on the warm side of the maximum (not shown). A weak mesohigh developed over southeastern New York into eastern Connecticut (Fig. 10b), the origins of which will be addressed in section 3b(3).

The 2-km WRF was able to reproduce the evolution of the surface temperature, wind, and pressure (Fig. 11). At 1800 UTC, the location of the model surface cold front was within 50 km of the observations (Figs. 10a and 11a), though the WRF had a weaker temperature gradient, with temperatures 1°–2°C too cool on the warm side of the baroclinic zone and 1°–2°C too warm on the cool side. At 2100 UTC, the model struggled to recreate mesoscale features, such as the mesohigh, though the location of the surface trough was within 50–75 km of the observed (Figs. 10b,11b). The WRF temperature gradient remained too weak, while surface dewpoints were 1°–2°C too low in the warm sector over the ocean (Figs. 11b).

2) INSTABILITY AND WIND PROFILE

At 1800 UTC, the QLCS was ~100 km northwest of the coastline (Fig. 1), moving southeastward into a region of moderate instability (WRF MUCAPE 1600–2000 J kg^{-1}; NARR MUCAPE 2000–2400 J kg^{-1}), which extended over the coastal waters (Figs. 12a,b). Surface-based instability was over Long Island Sound and the northern coast of Long Island (not shown). This is supported by the relatively shallow (300 m) inversion at JFK (Fig. 13a; see Fig. 1 for JFK location). This inversion was absent at locations farther north, such as LaGuardia Airport (LGA) (Figs. 4c,d; see Fig. 1 for location). At LGA, the atmosphere was almost dry adiabatic (~9°C km^{-1}) from the surface to 850 hPa in both the model sounding (Fig. 13e) and the ACARS-observed profile (Fig. 13f). At this time, there was weak 925-hPa warm air advection over the coast (Figs. 12a,b), with weak veering winds from the surface (south-southwest at 7.5 m s^{-1}) to 900 hPa (southwest at 13 m s^{-1}) at JFK (Fig. 13a) and no veering in the LGA profile within the deep, well-mixed boundary layer (Figs. 13c,d).

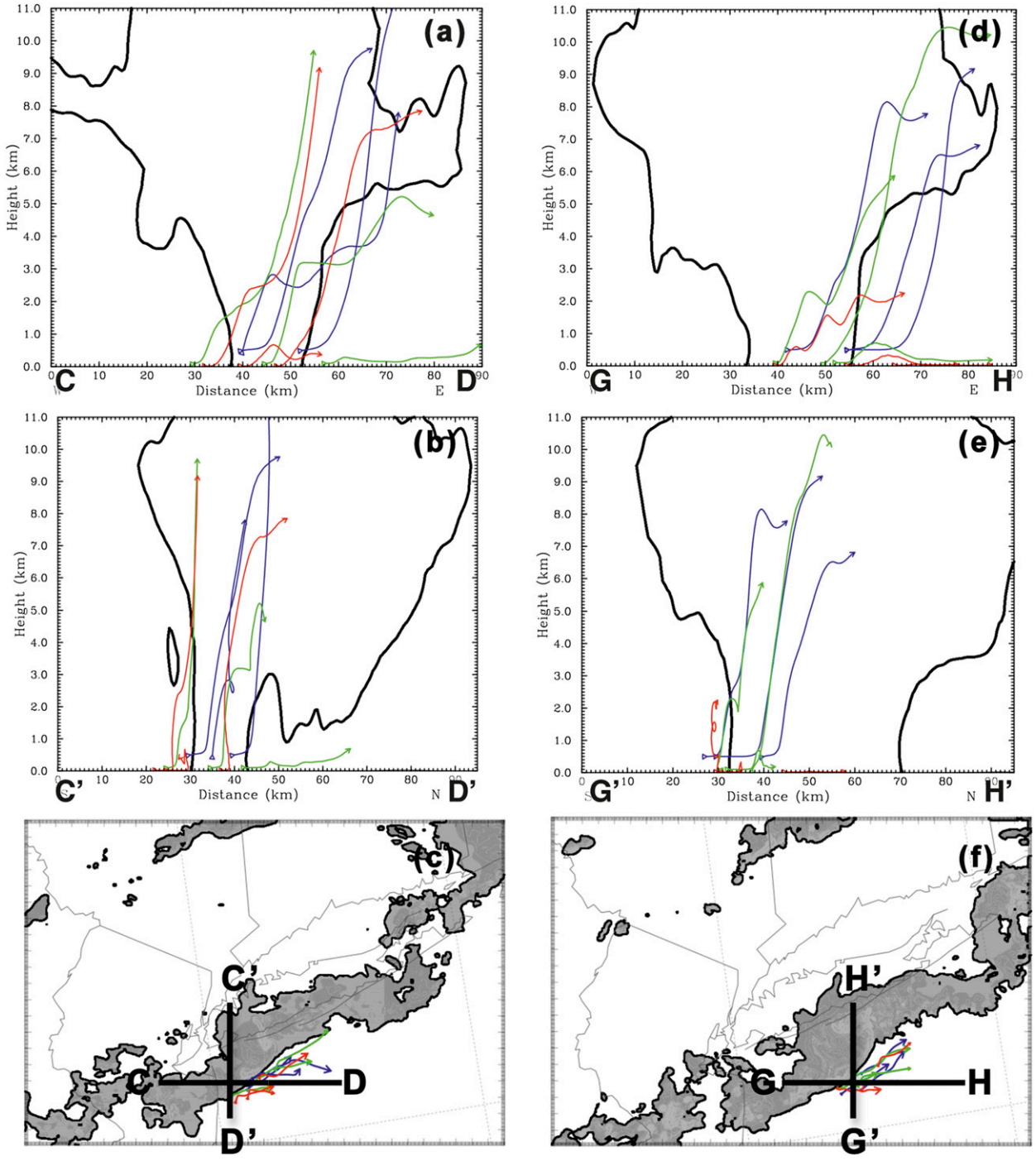

FIG. 8. (a) Cross section CD from the 500-m WRF domain showing 1-s forward trajectories interpolated from 30-s model output, released at 10 (red), 100 (green), and 500 m (blue) MSL launched at 0030 UTC (12.5 h) 1 Jun 2002 and run for 30 min with precipitation mixing ratio 0.64 g kg^{-1} contoured in black for 0030 UTC (12.5 h) 1 Jun 2002. (b) As in (a), but for cross section C′D′. (c) Horizontal projection of trajectories, with precipitation mixing ratio values ≥0.64 g kg^{-1} shaded in gray. (d) As in (a), but for trajectories released at 0100 UTC (13 h) for cross section GH. (e) As in (d), but for cross section G′H′. (f) As in (c), but for 0100 UTC (13 h). Location of cross sections CD, C′D′, GH, G′H′ marked with black solid line in (c),(f).

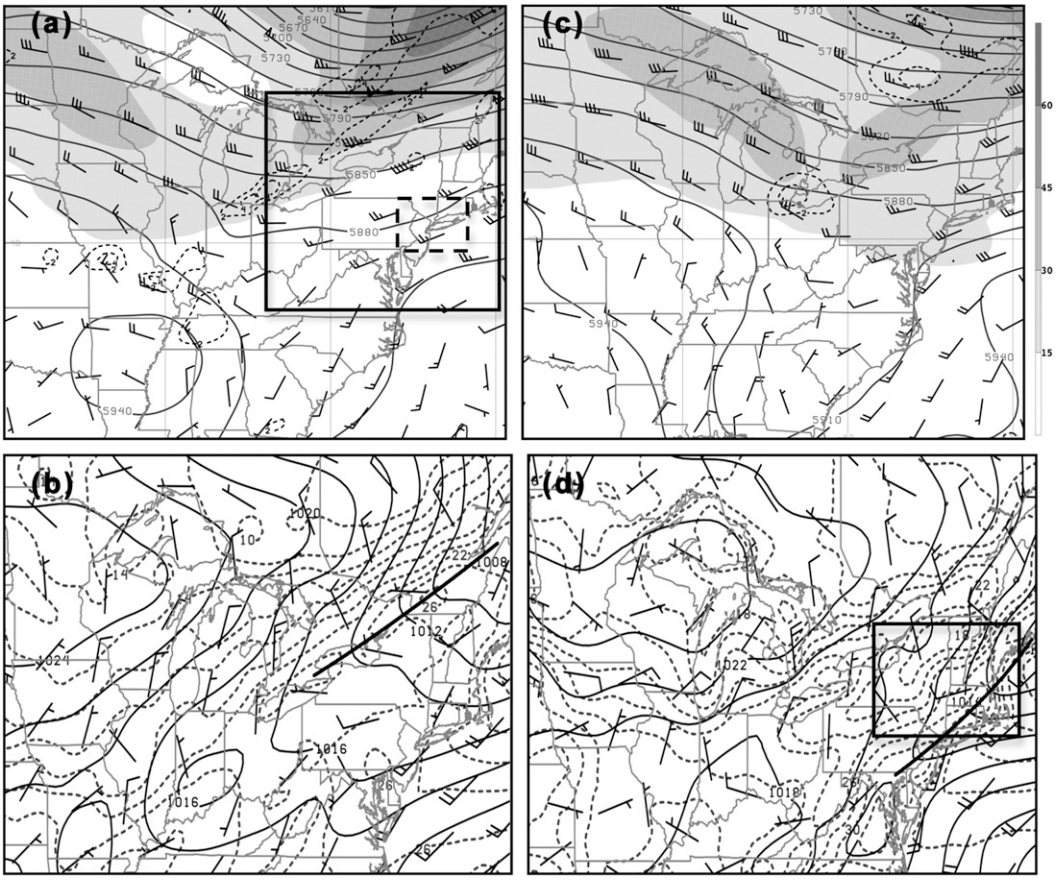

FIG. 9. The NARR (a) 300-hPa wind speed (shaded every 15 m s^{-1}), 500-hPa geopotential heights (solid every 30 dam), 500-hPa **Q**-vector convergence (dashed every 2×10^{-15} K m^{-2} s^{-1}), 500-hPa winds (full barb = 5 m s^{-1}) at 1200 UTC 23 Jul 2002. (b) As in (a), but for mean sea level pressure (solid every 2 hPa), 2-m temperature (dashed every 2°C), and 10-m winds (full barb = 5 m s^{-1}). (c) As in (a), but at 2100 UTC 23 Jul 2002. (d) As in (b), but at 2100 UTC 23 Jul 2002. The solid box (dashed box) in (a) marks the 2-km (500 m) WRF domain, and the box in (d) marks the location of the surface analysis in Fig. 10. The black solid line in (b),(d) marks the location of the surface cold front.

At 2100 UTC 23 July, MUCAPE was still available over the coastal waters ~50 km offshore of the mainland coast, with WRF MUCAPE values ranging 1200–1600 J kg^{-1} (Fig. 12c), ~400 J kg^{-1} less than the NARR (Fig. 12d). Surface-based instability remained closer to the coastline (not shown). Low-level (925 hPa) temperature advection was near neutral along the coast, with cold air advection associated with the surface cold front over the inland Northeast (Figs. 12c,d). At JFK, surface temperatures decreased 1°–2°C due to the decrease in diurnal heating, thus reinforcing the marine inversion (Fig. 13b). However, instability was present both inland and offshore during this event, indicating that a lack of ambient instability was not the reason this QLCS decayed upon encountering the coastline.

3) RADAR AND QLCS EVOLUTION

Figure 14 illustrates the observed and WRF radar reflectivity evolution of the 23 July 2002 decaying event as it approached the Atlantic waters. At 2016 UTC 23 July, the observed convective system was located 50–100 km to the northwest of the coastline, collocated with the surface cold front (Fig. 10b). Radar reflectivity values within the leading convective line approached 60 dBZ, with 50 dBZ within the trailing stratiform precipitation over New England (Fig. 14a). Within an hour, trailing stratiform precipitation developed behind the entire convective line, as the QLCS arrived at the coast (2215 UTC; Fig. 14b). The evaporative cooling associated with the region of trailing stratiform precipitation contributed to the development of the meso-high behind the cold front (Fig. 10b). Once offshore the leading convective line evolved into a line of cellular convection, with radar reflectivity values ~50 dBZ in the strongest cores (2215 UTC; Fig. 14c). By 0005 UTC 24 July, the decaying QLCS was ~60 km southeast of the mainland coast with no discernable organizational structure (Figs. 14d).

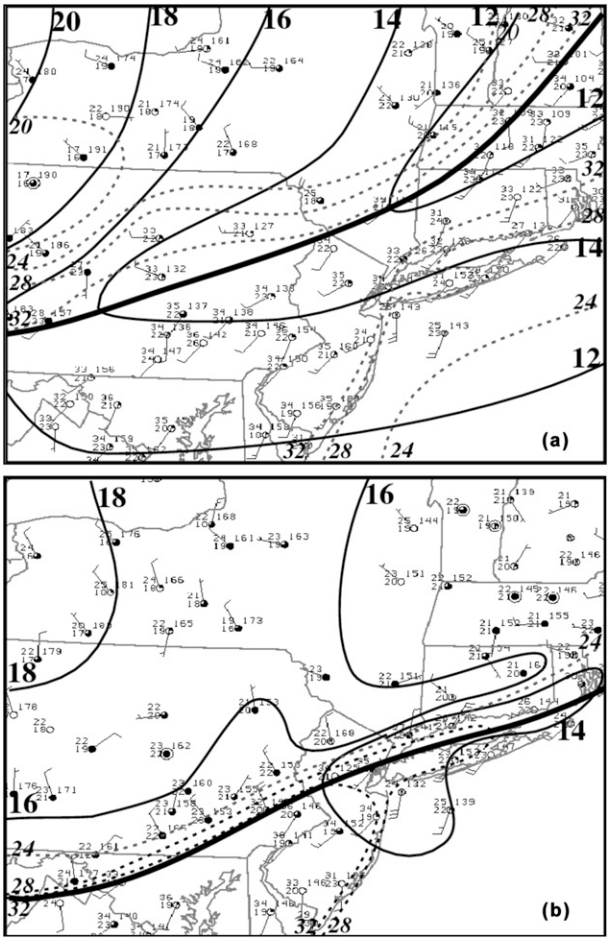

FIG. 10. Manual surface analysis at (a) 1800 UTC and (b) 2100 UTC 23 Jul 2002 showing MSLP (solid every 2 hPa), temperature (dashed every 4°C), dewpoint (°C), and winds (full barb = 10 kt). The location of the cold front is shown by the bold, solid line.

The 2-km and 500-m resolution WRF successfully reproduced the structure and evolution of the QLCS (Figs. 14e–h). At 2015 UTC, the location of the QLCS was within 50 km of observations, with a more north–south orientation compared to the observed (Figs. 14a,e), The simulated leading convective line and stratiform precipitation region was less organized than for the observed QLCS, potentially due to model spinup issues. The underdeveloped region of model stratiform precipitation at this time, as well as later in the evolution, likely contributed to the underdevelopment of the surface mesohigh in the model (Figs. 10b and 11b), since diabatic cooling processes were likely reduced behind the leading convective line. By 2115 UTC, the leading convective line was more continuous with a developing trailing stratiform rain region (Fig. 14f), though the WRF convection was ~20 km downstream of the observed. As the simulated QLCS moved over the coastal waters, it initially retained its linear characteristics (2200 UTC; Fig. 14g), though the system weakened substantially by 2300 UTC (Fig. 14h).

Cross sections were taken perpendicular to the movement of the QLCS, illustrated in Fig. 14f by line IJ, as it traversed the coastal boundary (Fig. 15). Cold pool parameters averaged over the 2-km-wide cross section were calculated using Eq. (1). At 2115 UTC 23 July, the QLCS was 5–10 km northwest of the marine layer, indicated by the cooler potential temperatures within the lowest levels to the southeast (Fig. 15a). At this time, the convective line was collocated with the leading edge of a 2.7 km (surface–700 hPa) deep cold pool (1.2 K θ_v'; Table 1) and the associated ascending motions of ~4 m s^{-1}. The LFC was ~850 hPa (~1.5 km), indicating that the cold pool was sufficient to lift parcels to saturation (not shown). The convection was moving into a region of conditional instability from the surface through 500–600 hPa (5–6 km; Fig. 15d).

By 2200 UTC, the QLCS was ~30 km southeast of the mainland coast over the marine layer (Fig. 15b). There was continued upward motion along the cold pool's leading edge, though the area of strongest ascent diminished (Fig. 15e), and the cold pool was ~3 km ahead of the convection (Fig. 15b). The ambient LFC remained near ~850 hPa, though within the cold pool it was much higher (~500 hPa; not shown). MUCAPE values ahead of the QLCS were 800–1400 J kg^{-1} (Figs. 12c,d), with SBCAPE values ranging 200–600 J kg^{-1} (not shown), which illustrates the availability of both surface and elevated instability. The 300-m-deep (surface–975 hPa) conditionally stable layer associated with the marine environment (Fig. 15e) highlights the more shallow inversion compared to the 31 May 2002 event. The 0–3-km storm-relative line-perpendicular vertical wind shear was 6–7 m s^{-1}, which is similar to the mean values of ambient 0–3-km shear for decaying QLCS events (7.4 m s^{-1}), as shown in Lombardo and Colle (2012). Within an hour (2300 UTC), the cold pool was ~15 km southeast of the decaying QLCS (Fig. 15c). There was little vertical motion along the leading edge of the cold pool at this time (Fig. 15f), with an ambient LFC at 800–750 hPa (2–2.5 km; not shown).

Forward 1-s trajectories highlight the source regions of air ingested into the QLCS as it moved out over the Atlantic waters (Fig. 16). As in the 31 May event, trajectories released at 10 (red), 100 (green), and 500 m (blue) are shown. At 2200 UTC, the QLCS was over the marine environment (Figs. 15b,c), though trajectories from all levels rose into the storm's updrafts (Figs. 16a,b). Within 30 min, a majority of the trajectories within the lowest 500 m (88%) and 100 m (93%) struggled to rise above 1–2 km, while all trajectories released at 10 m remained below 2 km (Figs. 16c,d). By 2300 UTC, no

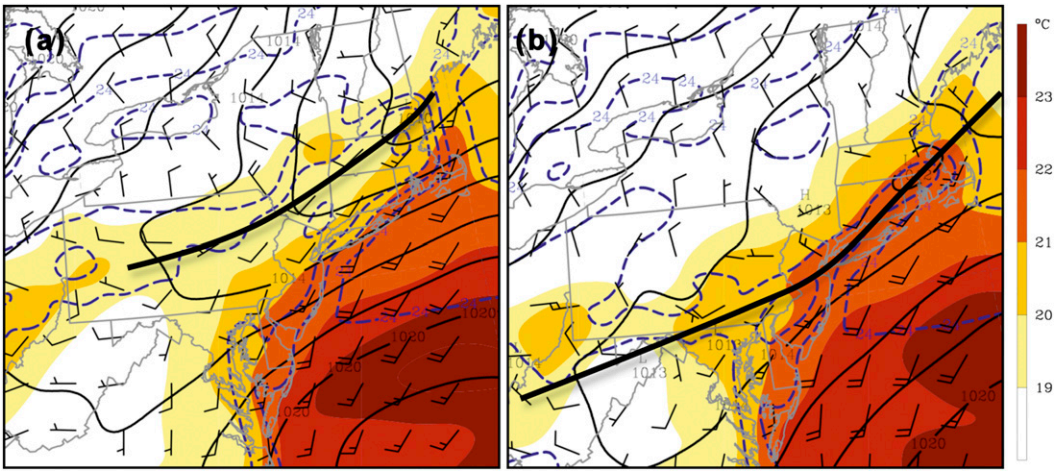

FIG. 11. 2-km WRF showing MSLP (solid every 2 hPa), 2-m temperature (dashed blue every 3°C), 2-m dewpoint (shaded every 1°C beginning at 19°C), and 10-m winds (full barb = 5 m s^{-1}) at (a) 1800 UTC and (b) 2100 UTC 23 Jul 2002. The location of the cold front is shown by the bold, solid line.

trajectories released at 10 and 100 m rose above 1 km, and those released at 500 m only rose to 2 km (Figs. 16e,f). At this time, only 5% of trajectories released at 2 km rose above 3 km (not shown). Those released ahead of the convective line though within the storm's outflow as well as those released ahead of the cold pool remained below the respective ambient LFCs as well. Therefore, as the QLCS evolved over the coastal waters, there was no indication of the storm becoming elevated (i.e., elevated parcels rising into the storm, while surface-based parcels remained within the boundary layer).

4. Discussion

a. Comparison between the 31 May and 23 July 2002 events

1) SYNOPTIC AND MESOSCALE ANALYSES

The 31 May QLCS was associated with stronger mid- and upper-level QG forcing (Figs. 2a,c) compared to the 23 July event (Figs. 9a,c), with regional synoptic forcing for ascent present during the sustaining QLCS event. However, the 23 July decaying QLCS was collocated with a surface cold front, which provided a mechanism for low-level ascent due to secondary frontogenetical circulations to support the convective line. Conversely, the 31 May sustaining QLCS was downstream of a surface cold front. Though this seems paradoxical, it is consistent with Lombardo and Colle (2012), who showed that one-quarter of decaying coastal QLCSs were collocated with a surface cold front, while no sustaining events were located along a cold front. Frontogenetical forcing is not required for a QLCS to successfully traverse the marine waters, and its presence does not guarantee the survival of organized convection over the marine layer.

Instability analyses illustrated the presence of offshore elevated (Fig. 12) and surface-based CAPE during the 23 July event, and elevated CAPE during the 31 May event (Fig. 4). Therefore, the intuitive assumption that a lack of instability over the coastal waters promotes convective decay does not apply to these events. For the 31 May event, parcels at and above 100 m (Fig. 8) were able to realize the offshore elevated CAPE and contribute to convective processes (Fig. 4). Workoff et al. (2012) showed a similar relationship for linear systems that successfully crossed Lake Erie. Organized storms had a greater chance of survival when the lake temperatures were cooler, limiting the amount of boundary layer air ingested into the storm.

2) STRENGTH OF COLD POOL AND VERTICAL WIND SHEAR

The above analyses suggest that cold pool dynamics may be important to the evolution and survival of the 31 May QLCS, since the system was not associated with any robust low-level features (i.e., cold front, mesolow). These processes may be important to the 23 July event as well, since the frontogenetical forcing was not sufficient to sustain the convective line. Previous literature has shown that in the absence of other forcing mechanisms, the maintenance of a QLCS may be governed by the strength of the diabatically generated cold pool in relation to the ambient vertical wind shear (i.e., Rotunno et al. 1988; Coniglio and Stensrud 2001; Weisman 1992). RKW theory (Rotunno et al. 1988) emphasized the

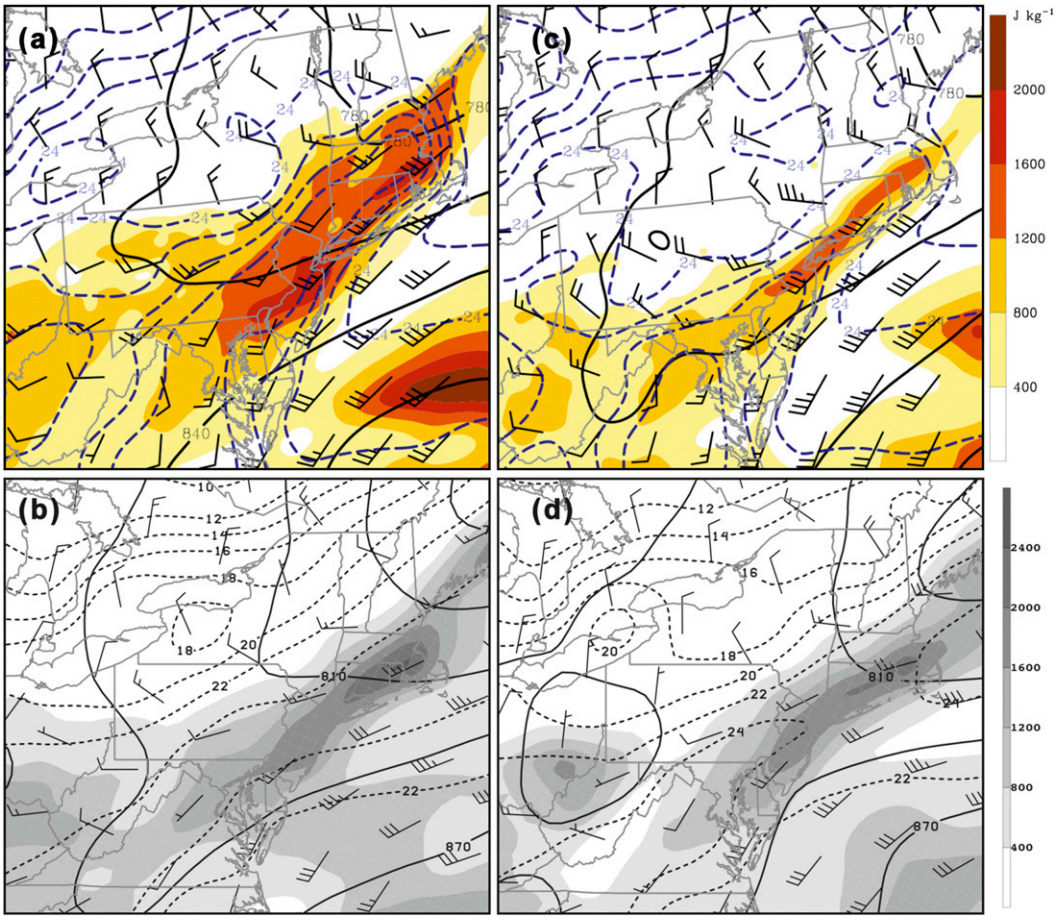

FIG. 12. (a) The 2-km WRF MUCAPE (shaded every 400 J kg^{-1}), 925-hPa geopotential heights (solid every 30 m), 925-hPa temperature (dashed every 2°C), and 925-hPa winds (full barb = 5 m s^{-1}) at 1800 UTC 23 Jul 2002. (b) NARR MUCAPE (shaded every 400 J kg^{-1}), 925-hPa geopotential heights (solid every 30 dam), 925-hPa temperature (dashed every 2°C), and 925-hPa winds (full barb = 5 m s^{-1}) at 1500 UTC 31 May 2002. (c) As in (a), but at 2100 UTC 23 Jul 2002. (d) As in (b), but at 2100 UTC 23 Jul 2002.

importance of line-perpendicular low-level wind shear (0–2.5 km; 0–3 km), stating that a balance between the horizontal vorticity induced by the low-level line-perpendicular winds and the horizontal vorticity generated by the QLCS density current favors upright mass evacuation at the leading edge of the cold pool and thus an upright, long-lived convective core. An "optimal" balance for deep lifting is achieved when the ratio of the theoretical strength of the cold pool c and the vertical wind shear downstream of the convective line Δu are ≈ 1 (Weisman and Rotunno 2004).

For both events, the $c/\Delta u$ relationship was calculated using θ_v', $\overline{\theta}_v$, and Δu averaged over the 2-km-wide cross section (Table 1). The theoretical speed of the cold pool was defined as

$$c^2 = -2\int_{z=0}^{z=H} B\,dz \qquad (1)$$

(i.e., Benjamin 1968; Rotunno et al. 1988; Weisman and Rotunno 2004; Bryan et al. 2006). The ambient line-perpendicular vertical wind shear was taken 50 km downstream of the leading edge of the cold pool (Table 1). Vertical shear values were also calculated 100 km downstream of the cold pool with little difference (not shown).

At 2345 UTC 31 May, prior to the QLCS interacting with the marine layer, the speed of the cold pool was 25.7 m s^{-1} with a line-perpendicular vertical wind shear value of 17.2 m s^{-1}, yielding a $c/\Delta u$ of 1.5. This is at the upper limit of the range of values indicating an upright convective system (Weisman and Rotunno 2004). At 0300 UTC 1 June, the ratio remained similar (i.e., 1.6) considering a surface based cold pool, though a modification to the calculation must be performed since the QLCS became elevated by this time, with the contribution of the cold pool to vertical lifting effectively zero below 200 m. Recent studies have suggested that the

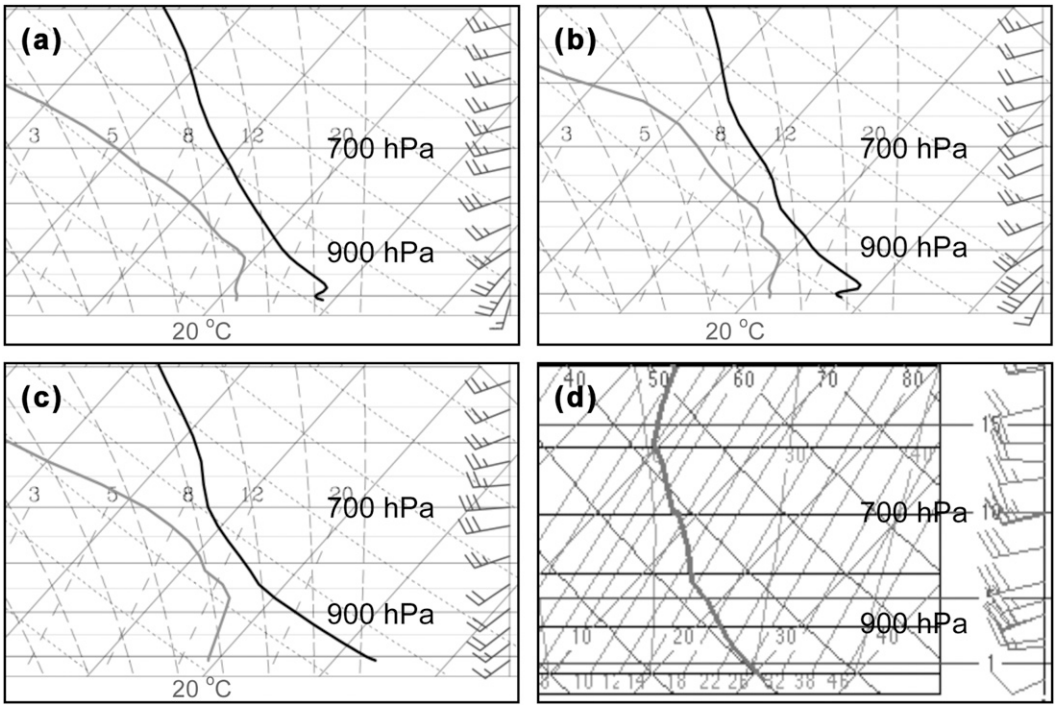

FIG. 13. WRF sounding from the 500-m domain at JFK at (a) 1800 UTC 23 Jul and (b) 2100 UTC 23 May, and (c) 1700 UTC 23 Jun 2002 at LGA. (d) As in (c), but for observed ACARS sounding at 1656 UTC 1 Jun 2002.

level over which the vertical wind shear is considered changes once a system becomes elevated. French and Parker (2010) argued that once a QLCS is no longer surface based, parcels within the lowest levels, which are within an area absent of CAPE, should no longer be considered in the problem since they are no longer involved in convective processes. The layer in which the horizontal gradients in cold pool buoyancy are maximized should be considered and subsequently only the wind shear within this elevated layer should be considered as well. Therefore, considering the layer in which $B < 0$ (200–2100 m), $c/\Delta u$ is 3.6, primarily due to a reduced vertical wind shear value (5.8 m s^{-1}), and it remained large (i.e., 3.0) 30 min later (Table 1). This is 3 times greater the theoretical optimal balance proposed by Weisman and Rotunno (2004). French and Parker (2010) hypothesized that as a QLCS becomes elevated and supported by an atmospheric bore above the stable layer, isentropic lift is sufficient enough to lift parcels to their LFC, since those parcels containing CAPE are above the surface, and thus require a small vertical displacement to convect freely. In this scenario, less vertical wind shear may be necessary to promote deep lifting along the leading edge of the elevated cold pool, though shear likely still contributes to the mechanism for ascent.

For the 23 July event, $c/\Delta u$ was ~1.5 (Table 1), falling within the range of values indicative of upright convection (Weisman and Rotunno 2004), as the QLCS was located over the inland side of the coastal boundary at 2115 UTC 23 July (Fig. 14f). This ratio increased to 2.7–2.9 (Table 1) as the QLCS moved over Long Island and the coastal waters, while the system remained surface based with $B < 0$ from the surface to H throughout the evolution. This is 2–3 times larger than the proposed optimal balance, indicating that conditions were suboptimal to support an upright convective core as the QLCS moved over Long Island and the Atlantic coastal waters. Since this system remained surface based, it was likely important to have robust vertical wind shear to assist in rigorous lifting along the leading edge of the cold pool, though shear values were relatively weak compared to the speed of the cold pool (Table 1).

b. Sensitivity tests

A series of sensitivity tests were performed using the WRF at 2-km grid spacing to test the importance of the magnitude of the cold pool and ambient vertical wind shear during each event.[1] The previous analysis suggests that the vertical wind shear was too weak during the 23 July event to promote upright mass evacuation at

[1] Performing these tests at 500-m resolution was too computationally expensive and not feasible.

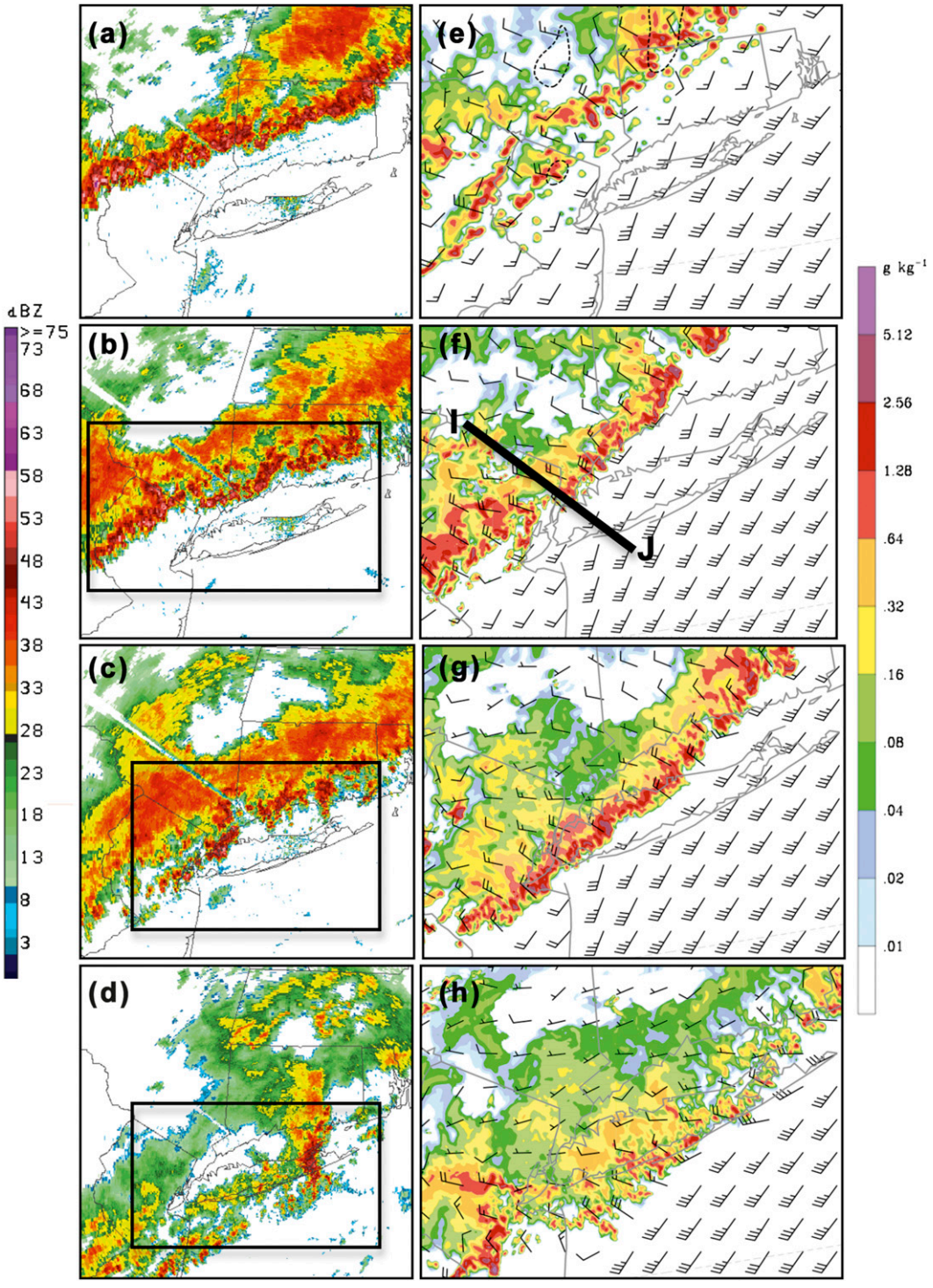

FIG. 14. Radar reflectivity from OKX at (a) 2016 UTC 23 Jul, (b) 2115 UTC 23 Jul, (c) 2215 UTC 23 Jul, and (d) 0005 UTC 24 Jul 2002. The WRF total precipitation mixing ratio ($g\,kg^{-1}$) and 100-m winds (full barb = $5\,m\,s^{-1}$) from (e) the 2-km domain at 2015 UTC 23 Jul (14.25 h), (f) 500-m domain at 2115 UTC (15.25 h) 23 Jul, (g) 500-m domain at 2200 UTC (16 h) 23 Jul, and (h) 500-m domain at 2300 UTC (17 h) 23 Jul. The box outline in (b)–(d) highlights the location of the WRF image in (f)–(h), respectively.

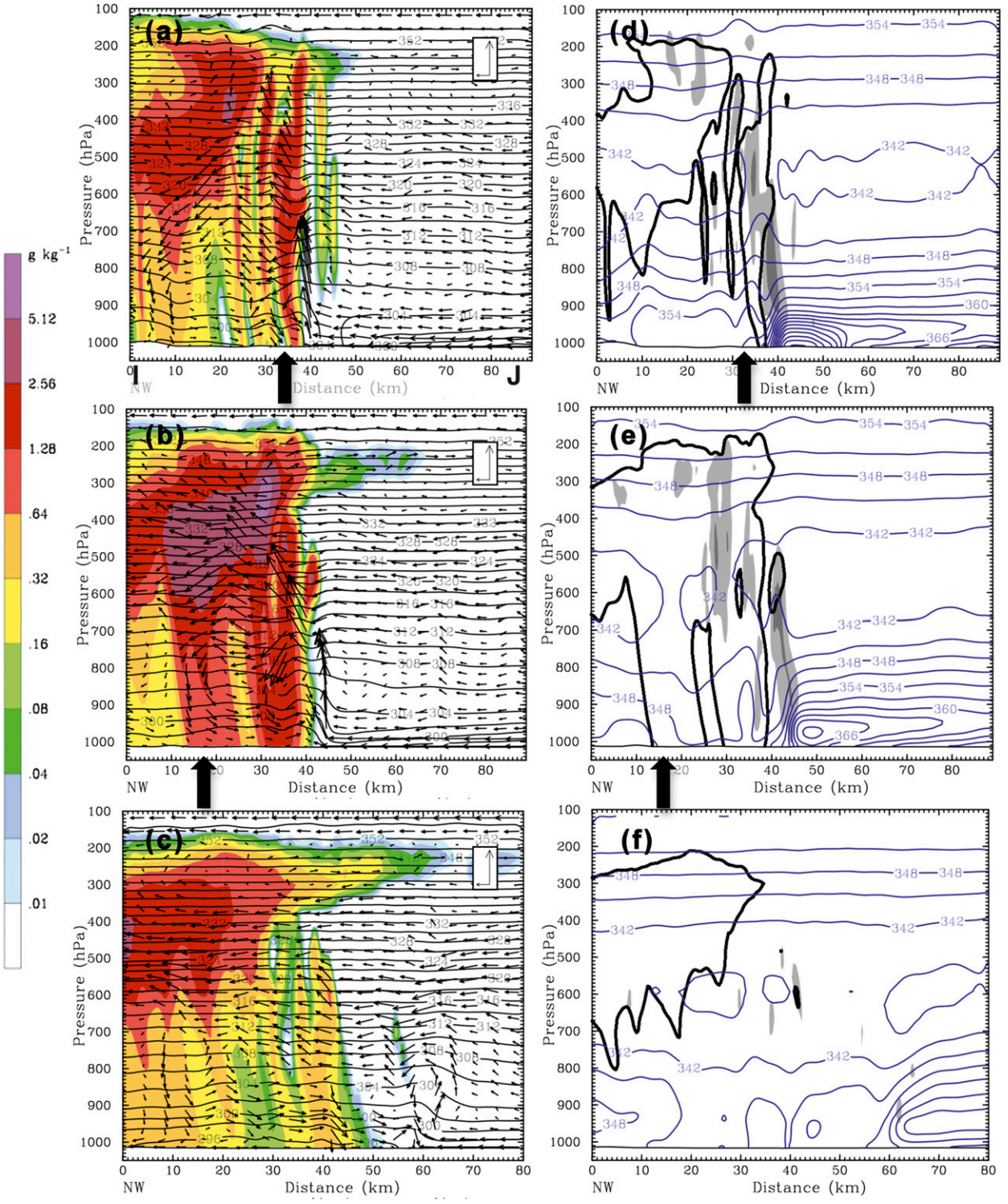

FIG. 15. 500-m WRF cross section IJ (labeled in Fig. 14f) averaged over 2-km width for 23 Jul 2002 at (a) 2115 UTC (15.25 h), (b) 2200 UTC (16 h), and (c) 2300 UTC (17 h). (a)–(c) Precipitation mixing ratio (shaded, g kg^{-1}), θ (black every 2 K), and storm-relative circulation vectors (storm motion southeast at 8.4 m s^{-1}) with the horizontal reference vector of 14 m s^{-1} and vertical reference vector of ~3.6 m s^{-1}. (d)–(f) Vertical motion (shaded every 3 m s^{-1}, beginning at 1 m s^{-1}), precipitation mixing ratio (black, 0.64 g kg^{-1}), and θ_{es} (blue every 3 K). The cross-sectional orientation is illustrated with a black line in Fig. 14f. Approximate location of the coastline is marked with an up arrow.

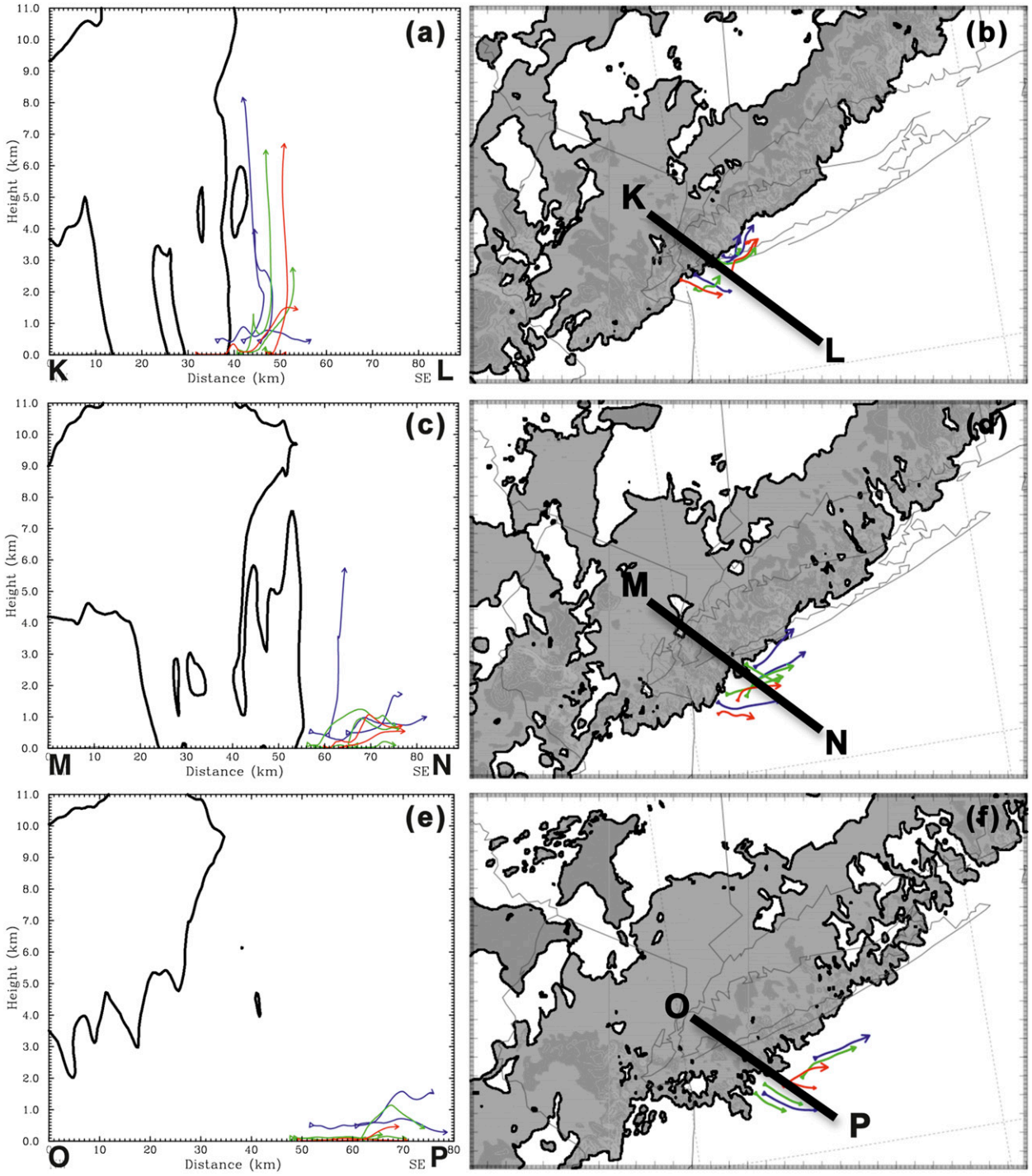

FIG. 16. (a) Cross section KL from the 500-m WRF domain showing 1-s forward trajectories interpolated from 30-s model output, released at 10 (red), 100 (green), and 500 m (blue) MSL launched at 2200 UTC (16 h) 23 Jul 2002 and run for 30 min with precipitation mixing ratio 0.64 g kg^{-1} contoured in black for 2200 UTC (16 h) 23 Jul 2002, (b) horizontal projection of trajectories, with precipitation mixing ratio values $\geq$0.64 g kg^{-1} shaded in gray. (c) As in (a), but for trajectories released at 2230 UTC (16.5 h) 23 Jul 2002 for cross section MN. (d) As in (b), but for 2230 UTC (16.5 h) 23 Jul 2002. (e) As in (a), but for trajectories released at 2300 UTC (17 h) for cross section OP. (f) As in (b), but for 2300 UTC (17 h) 23 Jul 2002. Location of cross sections KL, MN, and OP marked with black solid line in (b),(d),(f).

the leading edge of the cold pool. Hypothetically, if the QLCS was associated with a weaker and more shallow cold pool, the convection would have remained robust in the presence of weaker vertical wind shear. Since cold pools develop through diabatic cooling through evaporative processes, the evaporative cooling was reduced within the model to test this hypothesis.

The temperature tendency associated with melting and evaporation processes was reduced to 15% of the control simulation (EVAP15) beginning at 13 h (1900 UTC 23 July 2002) into the simulation, to reduce the development of the cold pool. Completely turning off evaporative cooling was attempted, but led to unrealistic solutions in the WRF (not shown). Other thresholds were tested (i.e., EVAP22, EVAP30) as well. The smaller reduction in evaporative cooling caused the QLCS to evolve in a similar manner to the EVAP15 simulation (EVAP22) or to decay similar to the CTRL (EVAP30).

During the 2-km CTRL experiment, the QLCS was located along the Atlantic coastline at 2200 UTC (Fig. 17a) and began to decay within an hour (Fig. 17b). By 0000 UTC, only the stratiform precipitation shield remained along the coast (Fig. 17c) with almost no precipitation visible by 0300 UTC (Fig. 17d).

For the EVAP15 experiment, 3 h after reducing the evaporative cooling, the QLCS was noticeably more organized and robust (Fig. 17e) compared to the CTRL at the same time (1600 UTC; Fig. 17a). By 1700 UTC, the EVAP15 QLCS was located along the Atlantic coast with precipitation mixing ratio values increasing along the entire line (Fig. 17f), though the QLCS moved more slowly southeastward compared to the CTRL (Fig. 17b). Three hours later (0200 UTC), the EVAP15 QLCS was located over the southern New England coast, with robust convection over northwestern Long Island (Fig. 17g), while the CTRL decayed 2 h prior (Fig. 17c). At this time, a mesocirculation began to develop over northeastern New Jersey as the QLCS was located over the coastline. By 0600 UTC, mesovortex was more defined as it moved over southern Long Island (Fig. 17h). The development of only a cyclonically rotating vortex resembles those documented by Atkins and St. Laurent (2009) as observed during the BAMEX experiment.

To more directly test the impact of the marine layer on the 23 July 2002 decaying QLCS, an experiment (LAND) was performed where the surface properties of the ocean were replaced with that of a forested area representative of the northeastern United States (Figs. 18 and 19). To accomplish this, several surface properties were modified at the start of the WRF simulation over the Atlantic Ocean, such as 1) the ocean was replaced with a deciduous broadleaf forest (similar to much of the northeastern United States) and 2) all surface and 2-m temperatures less than 293 K were set to 293 K to allow the surface temperatures over the coastal ocean to resemble the coastal land locations.

The LAND QLCS was located along the coastline at 2200 UTC 23 July (Fig. 18a), with slightly larger mixing ratio values than the CTRL (Fig. 17a). However, by 2300 UTC, the LAND QLCS began to decay as it moved over Long Island toward the Atlantic coastal waters (Fig. 18b), similar to the CTRL simulation (Fig. 17b). By 0000 UTC 24 July, the leading edge of the convective line decayed (Fig. 18c).

Introducing a land surface in place of the Atlantic marine environment led to several modifications of the ambient environment. In the LAND experiment, line-perpendicular winds within the lowest 400 m were 1–2 m s^{-1} more westerly, while winds within the 500–3000-m layer were up to 3 m s^{-1} more easterly (Fig. 19a), indicating that the vertical wind shear within the lowest few kilometers decreased, favoring the decay of the QLCS. Furthermore, the $c/\Delta u$ ratio at this time was 3.7, larger than for the CTRL QLCS (i.e., 2.7), primarily due to the reduction in vertical wind shear. While the speed of the cold pool was ~10% slower during the LAND experiment, the shear through the depth of the cold pool decreased by 30% (not shown), supporting the hypothesis that the reduction in shear promoted the decay of the convection.

The removal of the ocean also created an environment with a drier boundary layer, with a reduction in relative humidity values as much as 25%, though the atmosphere aloft became more saturated by 15% (Fig. 19b). Temperatures within the lowest 500-m layer increased as much as 6°C, while dewpoints decreased ~1°C (not shown). Between 500 and 3000 m, the dewpoints were as much as 5°C higher (not shown), contributing to an increase in relative humidity values. These thermodynamic changes lead to an increase in surface-based CAPE values of 400–800 J kg^{-1} ahead of the LAND QLCS (Fig. 19c), creating a thermodynamically more favorable environment for the maintenance of the QLCS. However, the QLCS decayed regardless of the larger instability, likely due to the reduction in low-level vertical wind shear.

These sensitivity tests further support the idea that cold pool dynamics were important in modulating the evolution of the convective systems, and the marine layer influence was likely secondary.

5. Summary

Two quasi-linear convective systems that encountered the Atlantic Ocean coastline within the New York City–Long Island region were explored in detail using high-resolution observations and numerical analyses to evaluate

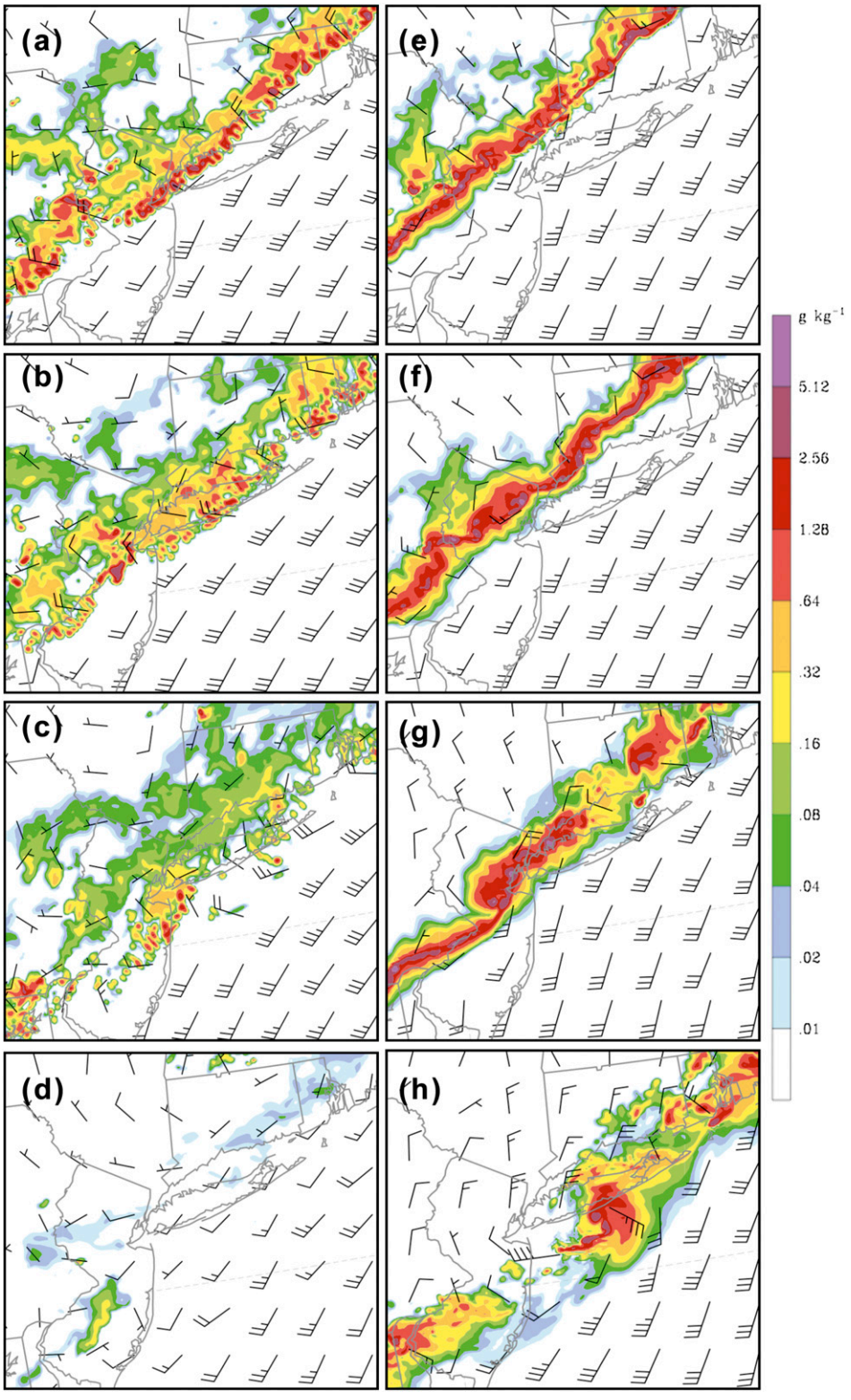

FIG. 17. 2-km WRF precipitation mixing ratio (shaded, g kg^{-1}) and 10-m winds (full barb = 5 m s^{-1}) for the control simulation (CTRL) at (a) (16 h) 2200 UTC 23 Jul, (b) (17 h) 2300 UTC 23 Jul, (c) (18 h) 0000 UTC 24 Jul, and (d) (21 h) 0300 UTC 24 Jul 2002. For the 15EVAP simulation at (e) (16 h) 2200 UTC 23 Jul, (f) (17 h) 2300 UTC 23 Jul, (g) (20 h) 0200 UTC 24 Jul, and (h) (24 h) 0600 UTC 24 Jul 2002.

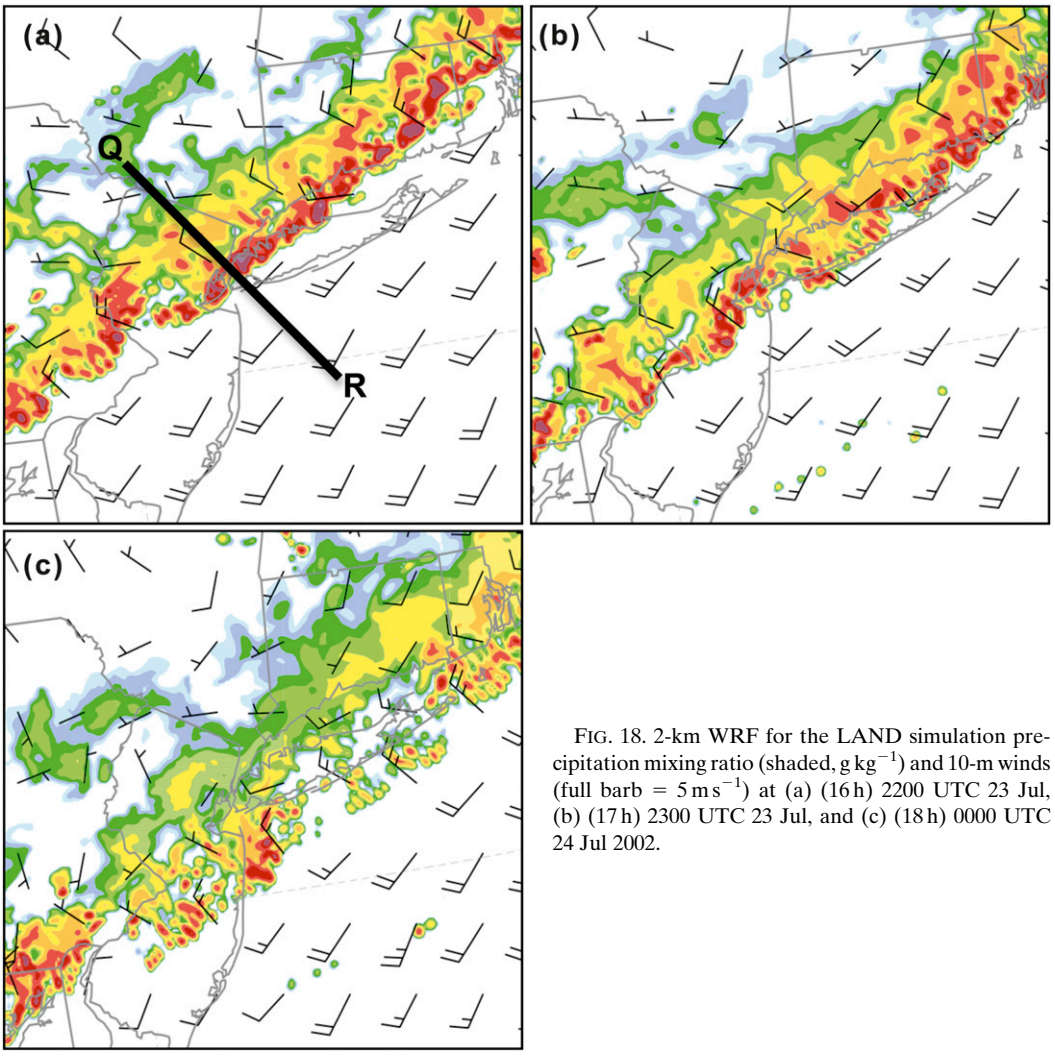

FIG. 18. 2-km WRF for the LAND simulation precipitation mixing ratio (shaded, g kg^{-1}) and 10-m winds (full barb = 5 m s^{-1}) at (a) (16 h) 2200 UTC 23 Jul, (b) (17 h) 2300 UTC 23 Jul, and (c) (18 h) 0000 UTC 24 Jul 2002.

the physical processes governing their evolutions. The 31 May 2002 no-stratiform QLCS event successfully traversed the marine waters just after 0000 UTC, while the 23 July 2002 trailing stratiform QLCS decayed upon reaching coast at ~2200 UTC.

During the 31 May event, there was evidence for modest mid- and upper-level QG forcing for ascent, indicated by 500-hPa **Q**-vector convergence as well as proximity of the region of interest to the exit region of an upper-level jet. At the surface, the QLCS was collocated with a prefrontal trough, ~200 km downstream of a surface cold front. Low-level warm air advection helped destabilize the coastal environment, increasing MUCAPE values to 400–1200 J kg^{-1}, as well as deepening the marine layer (750 m). The 0–3-km line-perpendicular wind shear over the marine waters was strong (15–20 m s^{-1}), which "balanced" the diabatically generated cold pool associated with the QLCS, promoting upright mass evacuation along the leading edge of the convective line, supporting convective initiation and development. Furthermore, as the QLCS moved offshore and encountered the marine inversion, the surface based system became slightly elevated, though not above the boundary layer.

For the 23 July event, there was little mid- and upper-level forcing for ascent to support the convective line, though the convection was collocated with a robust surface cold front. The QLCS encountered the coastline while organized along the frontal boundary, though it decayed regardless. There was limited low-level temperature advection over the QLCS, though instability values (MUCAPE 1200–1600 J kg^{-1}) during this event were greater than the 31 May sustaining event. However, the 0–3-km line-perpendicular wind shear over the ocean was only 6–7 m s^{-1}, less than half of that during the 31 May event. The cold pool overwhelmed this relatively weak vertical wind shear, and moved

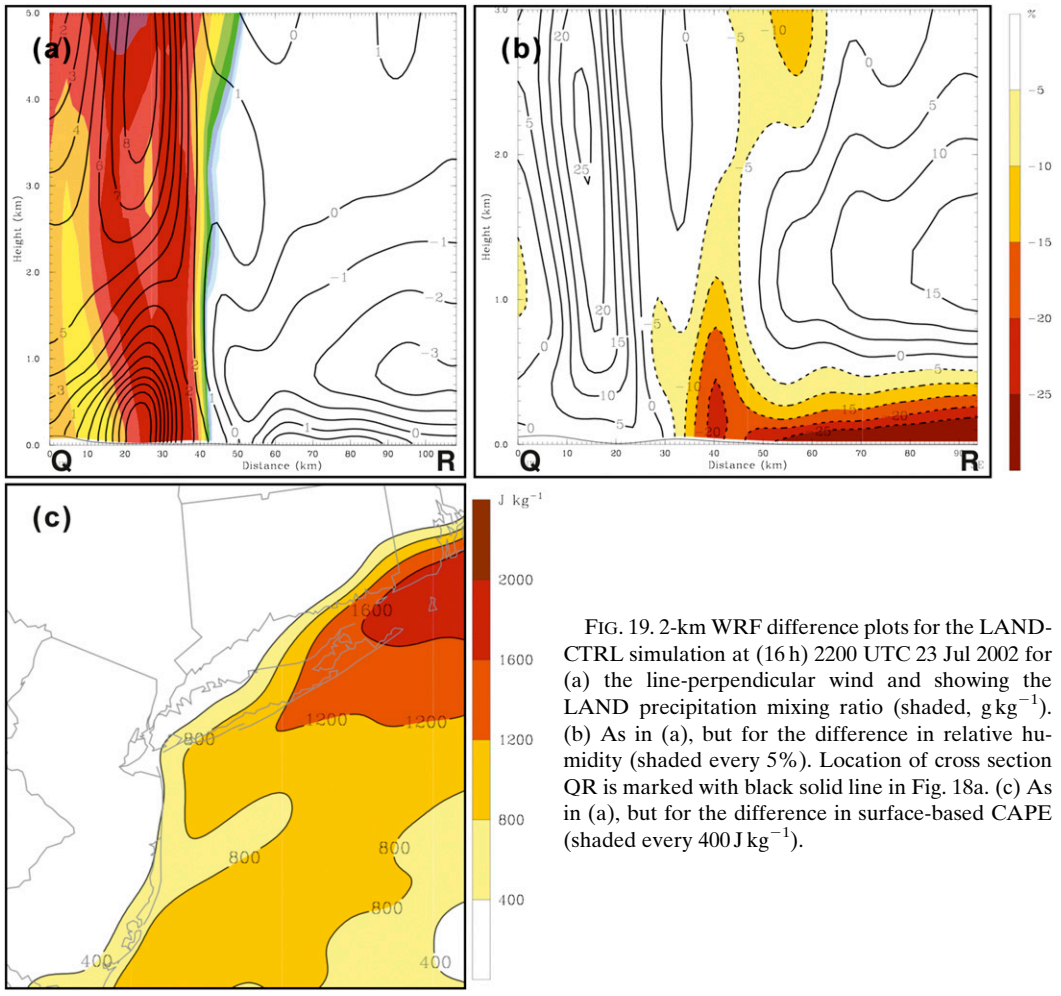

FIG. 19. 2-km WRF difference plots for the LAND-CTRL simulation at (16 h) 2200 UTC 23 Jul 2002 for (a) the line-perpendicular wind and showing the LAND precipitation mixing ratio (shaded, g kg^{-1}). (b) As in (a), but for the difference in relative humidity (shaded every 5%). Location of cross section QR is marked with black solid line in Fig. 18a. (c) As in (a), but for the difference in surface-based CAPE (shaded every 400 J kg^{-1}).

ahead of the convective line, leading to the decay of the storm.

Numerical sensitivity experiments emphasized the importance of cold pool dynamics in governing the life cycle of the linear systems, and highlighted the lesser importance of the Atlantic marine layer during these two events. For the 23 July decaying QLCS, a reduction in diabatic cooling, thus the development of the cold pool, lead to a more robust QLCS that successfully moved over the Atlantic waters. When the ocean was replaced by a land surface for the 23 July event, effectively removing the presence of a marine layer, the QLCS decayed regardless. While the ambient surface based CAPE increased by 400–800 J kg^{-1} during this experiment, the further reduction in vertical wind shear by the insertion of the land surface promoted the decay of the 23 July QLCS.

This paper highlights the complexities influencing the evolution of a QLCS encountering a coastal marine environment. Analysis of additional case studies would provide further insight into the role of the marine layer during these events. Furthermore, approaching this problem using idealized numerical experiments would allow one to isolate the role of the various factors discussed above and evaluate their importance individually.

Acknowledgments. The authors thank Dr. Matthew Parker, as well as reviewers Dr. Russ Schumacher and Dr. Tom Galarneau for their insightful comments that helped improve and shape the manuscript. This study was supported by the National Science Foundation under Grant ATM-0705036.

REFERENCES

Ahijevych, D. A., C. A. Davis, R. E. Carbone, and J. D. Tuttle, 2004: Initiation of precipitation episodes relative to elevated terrain. *J. Atmos. Sci.,* **61,** 2763–2769.

Atkins, N. T., and M. St. Laurent, 2009: Bow echo mesovorticies. Part II: Their genesis. *Mon. Wea. Rev.,* **137,** 1514–1532.

Benjamin, T. B., 1968: Gravity currents and related phenomena. *J. Fluid Mech.,* **31,** 209–248.

Bosart, L. F., and F. Sanders, 1981: The Johnstown flood of July 1977: A long-lived convective system. *J. Atmos. Sci.,* **38,** 1616–1642.

——, and T. J. Galarneau Jr., 2005: The influence of the Great Lakes on warm season weather systems during BAMEX. Preprints, *Sixth Conf. on Coastal Atmospheric and Oceanic Prediction and Processes,* San Diego, CA, Amer. Meteor. Soc., 3.5. [Available online at https://ams.confex.com/ams/Annual2005/techprogram/paper_84665.htm.]

Bryan, G. H., C. K. Jason, and M. D. Parker, 2006: A multimodel assessment of RKW Theory's relevance to squall-line characteristics. *Mon. Wea. Rev.,* **134,** 2772–2792.

Carbone, R. E., J. D. Tuttle, D. A. Ahijevych, and S. B. Trier, 2002: Inferences of predictability associated with warm season precipitation episodes. *J. Atmos. Sci.,* **59,** 2033–2056.

Changnon, S. A., 1980: Evidence of urban and lake influences on precipitation in the Chicago area. *J. Appl. Meteor.,* **19,** 1137–1159.

Coniglio, M. C., and D. J. Stensrud, 2001: Simulation of a progressive derecho using composite initial conditions. *Mon. Wea. Rev.,* **129,** 1593–1616.

——, ——, and M. B. Richman, 2004: An observational study of derecho-producing convective systems. *Wea. Forecasting,* **19,** 320–337.

——, ——, and L. J. Wicker, 2006: Effects of upper-level shear on the structure and maintenance of strong quasi-linear mesoscale convective systems. *J. Atmos. Sci.,* **63,** 1231–1252.

Davis, C., and Coauthors, 2004: The bow echo and MCV experiment: Observations and opportunities. *Bull. Amer. Meteor. Soc.,* **85,** 1075–1093.

Doswell, C. A., III, and J. S. Evans, 2003: Proximity sounding analysis for derechos and supercells: An assessment of similarities and differences. *Atmos. Res.,* **67–68,** 117–133.

Frame, J., and P. Markowski, 2006: The interaction of simulated squall lines with idealized mountain ridges. *Mon. Wea. Rev.,* **134,** 1919–1941.

French, A. J., and M. D. Parker, 2010: The response of simulated nocturnal convective systems to a developing low-level jet. *J. Atmos. Sci.,* **67,** 3384–3408.

Hong, S.-Y., Y. Noh, and J. Dudhia, 2006: A new vertical diffusion package with an explicit treatment of entrainment processes. *Mon. Wea. Rev.,* **134,** 2318–2341.

Janjic, Z. I., 1990: The step-mountain coordinate: Physical package. *Mon. Wea. Rev.,* **118,** 1429–1443.

Lericos, T. P., H. E. Fuelberg, M. L. Weisman, and A. I. Watson, 2007: Numerical simulations of the effects of coastlines on the evolution of strong, long-lived squall lines. *Mon. Wea. Rev.,* **135,** 1710–1731.

Letkewicz, C. E., and M. D. Parker, 2010: Forecasting the maintenance of mesoscale convective systems crossing the Appalachian Mountains. *Wea. Forecasting,* **25,** 1179–1195.

——, and ——, 2011: Impact of environmental variations on simulated squall lines interacting with terrain. *Mon. Wea. Rev.,* **139,** 3163–3183.

Lombardo, K. A., and B. A. Colle, 2010: The spatial and temporal distribution of organized convective structures over the Northeast and their ambient conditions. *Mon. Wea. Rev.,* **138,** 4456–4474.

——, and ——, 2012: Ambient conditions associated with the maintenance and decay of quasi-linear convective systems crossing the northeastern U.S. coast. *Mon. Wea. Rev.,* **140,** 3805–3819.

Mapes, B. E., T. T. Warner, M. Xu, and A. J. Negri, 2003: Diurnal patterns of rainfall in northwestern South America. Part I: Observation and context. *Mon. Wea. Rev.,* **131,** 799–811.

Mesinger, F., and Coauthors, 2006: North American Regional Reanalysis. *Bull. Amer. Meteor. Soc.,* **87,** 343–360.

Metz, N. D., 2011: Persistence and dissipation of Lake Michigan-crossing mesoscale convective systems. Ph.D. dissertation, University at Albany, State University of New York, 237 pp.

Miglietta, M. M., and R. Rotunno, 2009: Numerical simulations of conditionally unstable flows over a mountain ridge. *J. Atmos. Sci.,* **66,** 1865–1885.

Morrison, H., G. Thompson, and V. Tatarskii, 2009: Impact of cloud microphysics on the development of trailing stratiform precipitation in a simulated squall line: Comparison of one- and two-moment schemes. *Mon. Wea. Rev.,* **137,** 991–1007.

Murray, J. C., and B. A. Colle, 2011: The spatial and temporal variability of convective storms over the northeast United States during the warm season. *Mon. Wea. Rev.,* **139,** 992–1012.

Nakanishi, M., and H. Niino, 2006: An improved Mellor–Yamada level-3 model: Its numerical stability and application to a regional prediction of advection fog. *Bound.-Layer Meteor.,* **119,** 397–407.

Parker, M. D., 2008: Response of simulated squall lines to low-level cooling. *J. Atmos. Sci.,* **65,** 1323–1341.

——, and R. H. Johnson, 2000: Organizational modes of midlatitude mesoscale convective systems. *Mon. Wea. Rev.,* **128,** 3413–3436.

——, and D. A. Ahijevych, 2007: Convective episodes in the east-central United States. *Mon. Wea. Rev.,* **135,** 3707–3727.

Reeves, H. D., and Y.-L. Lin, 2007: The effects of a mountain on the propagation of a preexisting convective system for blocked and unblocked flow regimes. *J. Atmos. Sci.,* **64,** 2401–2421.

Rotunno, R., J. B. Klemp, and M. L. Weisman, 1988: A theory for strong, long-lived squall lines. *J. Atmos. Sci.,* **45,** 463–485.

Skamarock, W. C., and Coauthors, 2008: A description of the Advanced Research WRF version 3. NCAR Tech. Note NCAR/TN-475+STR, 125 pp.

Trier, S. B., C. A. Davis, D. A. Ahijevych, M. L. Weisman, and G. H. Bryan, 2006: Mechanisms supporting long-lived episodes of propagating nocturnal convection within a 7-day WRF model simulation. *J. Atmos. Sci.,* **63,** 2437–2461.

Weisman, M. L., 1992: The role of convectively generated rear-inflow jets in the evolution of long-lined mesoconvective systems. *J. Atmos. Sci.,* **49,** 1826–1847.

——, and J. Klemp, 1982: The dependence of numerically simulated convective storms on vertical wind shear and buoyancy. *Mon. Wea. Rev.,* **110,** 504–520.

——, and R. Rotunno, 2004: ''A theory for strong long-lived squall lines'' revisited. *J. Atmos. Sci.,* **61,** 361–382.

——, J. B. Klemp, and R. Rotunno, 1988: Structure and evolution of numerically simulated squall lines. *J. Atmos. Sci.,* **45,** 1990–2013.

Workoff, T., 2010: A study of the effect of Lake Erie on deep convective systems. M.S. thesis, University of Illinois at Urbana–Champaign, Urbana, IL, 95 pp.

——, D. A. R. Kristovish, N. F. Laird, R. LaPlante, and D. Leins, 2012: Influence of the Lake Erie overlake boundary layer on deep convective storm evolution. *Wea. Forecasting,* **27,** 1279–1289.